Müzeyyen SAVAŞ

A Master's Thesis

AGU 2022

FABRICATION AND NOVEL APPLICATIONS OF LIGHT-ABSORBING OPTOELECTRONIC DEVICES

A THESIS
SUBMITTED TO THE DEPARTMENT OF ELECTRICAL AND COMPUTER ENGINEERING
AND THE GRADUATE SCHOOL OF ENGINEERING AND SCIENCE
OF ABDULLAH GUL UNIVERSITY
IN PARTIAL FULFILLMENT OF THE REQUIREMENTS
FOR THE DEGREE OF
MASTER OF SCIENCE

By
Müzeyyen Savaş
August 2022

FABRICATION AND NOVEL APPLICATIONS OF LIGHT-ABSORBING OPTOELECTRONIC DEVICES

A THESIS
SUBMITTED TO THE DEPARTMENT OF ELECTRICAL AND COMPUTER ENGINEERING
AND THE GRADUATE SCHOOL OF ENGINEERING AND SCIENCE OF ABDULLAH GUL UNIVERSITY
IN PARTIAL FULFILLMENT OF THE REQUIREMENTS
FOR THE DEGREE OF
MASTER OF SCIENCE

By
Müzeyyen Savaş
August 2022

SCIENTIFIC ETHICS COMPLIANCE

I hereby declare that all information in this document has been obtained in accordance with academic rules and ethical conduct. I also declare that, as required by these rules and conduct, I have fully cited and referenced all materials and results that are not original to this work.

Name-Surname: Müzeyyen Savaş
Signature :

REGULATORY COMPLIANCE

M.Sc. thesis titled Fabrication and Novel Applications of Light-Absorbing Optoelectronic Devices has been prepared in accordance with the Thesis Writing Guidelines of the Abdullah Gül University, Graduate School of Engineering & Science.

Prepared By	Advisor
Müzeyyen Savaş	Asst. Prof. Talha Erdem

Head of the Electrical and Computer Engineering Program

Assoc. Prof. Kutay İçöz

ACCEPTANCE AND APPROVAL

M.Sc. thesis titled Fabrication and Novel Applications of Light-Absorbing Optoelectronic Devices and prepared by Müzeyyen Savaş has been accepted by the jury in the Electrical and Computer Engineering Graduate Program at Abdullah Gül University, Graduate School of Engineering & Science.

08/08/2022

(Thesis Defense Exam Date)

JURY:

Advisor : Asst. Prof. Talha Erdem

Member : Assoc. Prof. Kutay İçöz

Member : Prof. M. Serdar Önses

APPROVAL:

The acceptance of this M.Sc. thesis has been approved by the decision of the Abdullah Gül University, Graduate School of Engineering & Science, Executive Board dated ….. /….. / …….. and numbered ……..……. .

…….. /…….. / ……..

(Date)

Graduate School Dean
Prof. Dr. İrfan ALAN

ABSTRACT

FABRICATION AND NOVEL APPLICATIONS OF LIGHT-ABSORBING OPTOELECTRONIC DEVICES

Müzeyyen Savaş
MSc. in Electrical and Computer Engineering
Advisor: Asst. Prof. Talha Erdem

August 2022

Fabrication of optoelectronic devices relies on expensive, energy-consuming conventional tools including chemical vapor deposition, lithography, and metal evaporation. Developing an alternative technology would contribute to the efforts on achieving a sustainable optoelectronics technology. Keeping this in our focus, here we present a simple technique to fabricate visible photodetectors. These fully solution-processed and transparent metal-semiconductor-metal photodetectors employ silver nanowires (Ag NW) as the transparent electrodes replacing the indium-tin-oxide (ITO) commonly used in optoelectronic devices. By repeatedly spin coating Ag NW on a glass substrate followed by the coating of ZnO nanoparticles, we obtained a highly conductive transparent electrode reaching a sheet resistance of 95 Ω/□. The transmittance of the Ag NW-ZnO films was 84% at 450 nm while the transmittance of the ITO films was 90% at the same wavelength. Following the formation of the conductive film, we scratched it using a heated surgical blade to open a gap which is ~30 μm forming an insulating line. As the active layer, we drop-casted red-emitting CdSe/ZnS core-shell colloidal quantum dots (CQDs) onto this gap. These visible CQD-based photodetectors exhibited responsivities and detectivities up to 8.5 mA/W and 0.95×10^9 Jones, respectively. These proof-of-concept photodetectors show that the environmentally friendly, low-cost, and energy-saving technique presented here can be an alternative to conventional, high-cost, and energy-hungry techniques while fabricating light-harvesting devices.

Keywords:colloidal quantum dot photodetectors, zinc oxide nanoparticles, silver nanowires, sustainable fabrication, sustainable optoelectronics.

ÖZET

IŞIK EMİCİ OPTOELEKTRONİK CİHAZLARIN ÜRETİMİ VE YENİ UYGULAMALARI

Müzeyyen Savaş
Elektrik ve Bilgisayar Mühendisliği Anabilim Dalı Yüksek Lisans
Tez Yöneticisi: Dr. Öğr. Üyesi Talha Erdem

Ağustos-2022

Optoelektronik cihazların üretimi, kimyasal buhar kaplama, litografi ve metal buharlaştırma dahil olmak üzere pahalı, enerji tüketen geleneksel araçlara dayanır. Alternatif bir teknolojinin geliştirilmesi, sürdürülebilir bir optoelektronik teknolojisine ulaşma çabalarına katkıda bulunacaktır. Bunu odak noktamızda tutarak, burada görünür fotodedektörleri imal etmek için basit bir teknik sunuyoruz. Bu tamamen çözelti ile işlenmiş ve şeffaf metal-yarı iletken-metal fotodedektörler, optoelektronik cihazlarda yaygın olarak kullanılan indiyum-kalay oksitin (ITO) yerini alan şeffaf elektrotlar olarak gümüş nanotelleri (Ag NW) kullanmıştır. Bir cam substrat üzerinde Ag NW'leri tekrar tekrar döndürerek kaplamayı takiben ZnO nanoparçacıklarının kaplanmasıyla, 95 Ω/□'lik bir tabaka direncine ulaşan oldukça iletken şeffaf bir elektrot elde edilmiştir. Ag NW-ZnO filmlerinin geçirgenliği 450 nm'de %84 iken, aynı dalga boyunda ITO filmlerinin geçirgenliği %90 olmuştur. İletken filmin oluşumunu takiben, bir yalıtım hattı oluşturan ~30 μm'lik bir boşluk açmak için ısıtılmış bir cerrahi bıçak kullanarak film çizilmiştir. Aktif katman olarak, bu boşluğa kırmızı yayan CdSe/ZnS çekirdek-kabuk kolloidal kuantum noktalarını (KKN'ler) damlatılmıştır. Bu görünür KKN tabanlı fotodedektörler, sırasıyla 8.5 mA/W ve 0.95×10^9 Jones'a kadar duyarlılık ve algılama sergilemiştir. Bu kavram kanıtı fotodedektörler, burada sunulan çevre dostu, düşük maliyetli ve enerji tasarruflu tekniğin, ışık hasat eden cihazları üretirken geleneksel, yüksek maliyetli ve çok enerji tüketen tekniklere bir alternatif olabileceğini göstermektedir.

Anahtar kelimeler: kolloidal kuantum nokta fotodedektörler, çinko oksit nanopartiküller, gümüş nanoteller, sürdürülebilir üretim, sürdürülebilir optoelektronik.

Acknowledgements

As one of the major milestones of my life, herewith I have finished my M.Sc. with this thesis. During this period of my life, I have met a lot of people and I have learned a lot of things from them. I owe many thanks to all of them.

First, I would like to express my deepest gratitude to my advisor Asst. Prof. Talha Erdem. I was lucky to be able to work under him as I got the chance to improve myself by learning from him, from his experiences and from his never-ending guidance. He helped and supported me in every part of my graduate study.

I would also like to thank Prof. Evren Mutlugün, who has supported and helped me during my master. In addition, I owe many thanks to Assoc. Prof. Kutay İçöz for his support during my master. Finally, I would like to thank Prof. M. Serdar Önses for accepting to be in my thesis committee.

At this point, I, of course, thank my family: My father and mother, for their supports and patience, and for many things that I cannot put into words. Also, I owe many thanks to my brothers that have been with me whenever I need them.

In my work, there were times when I needed help with getting certain materials or understanding a concept or even a procedure that I couldn’t understand and I was lucky to be with students, teaching assistants and research assistants of AGU who were always helping with a smile, to name a few, Ahmet Faruk Yazıcı, Ayşenur Arslan, Zeynep Şenel, Muhammad Fuad Farooqi, and Ruby Phul.

Finally, I would like to thank TUBITAK (project no. 20AG026) for the financial support.

TABLE OF CONTENTS

LIST OF FIGURES

LIST OF TABLES

LIST OF ABBREVIATIONS

Ag NW	Silver Nonaowires
ZnO NP	Zinc Oxide Nanoparticles
CQDs	Colloidal Quantum Dots
PD	Photodetector
EHP	Electron-Hole Pair
SJ	Schottky Junction
ITO	Indium Tin Oxide

To my parents for their absolute love,
support and motivation

Chapter 1

Introduction

This thesis is based on the conference paper that accepted in the SPIE Europe proceeding [1].

Photodetectors (PDs) are among the most widely used optoelectronic devices that find various applications in a variety of fields including commercial electronics [2], imaging [3], communications [4], and military equipment [5]. Such diverse applications bring together the need for certain specifications depending on the purpose of use. For example, infrared photodetectors are very critical for military applications [6] whereas civil cameras must work in the visible regime [7]. Similarly, the photodetectors used by the telecommunications industry must be very fast [8] whereas the photodetectors used for lighting applications do not require such high speeds. Such differences in the application requirements triggered the use of various active region materials [9] as well as device architectures [10].

Fabrication of these photodetectors relies on conventional tools such as chemical vapor deposition, lithography, and metal evaporation [11]–[13]. These tools and techniques are expensive, energy-consuming and employ toxic chemicals [14]. Furthermore, the thin films in these devices are usually deposited at elevated temperatures and under high vacuum which impose further restrictions on the device fabrication. Along with their increased energy consumption, the fabrication process of the photodetectors, like most the other electronic and optoelectronic devices, has benign effects on the environment.

The attempts to decrease the environmental footprint of the optoelectronic device fabrication should involve the materials within the active region and the electrodes. Silicon and germanium step forward as the most widely used semiconductors used in the active region of the photodetectors [15]. However, their growth process is far from being environmentally friendly [16]. An alternative to them is using solution-processed materials that most of the time simply require a spin-coating process. For this purpose, perovskites [17], colloidal quantum dots (QDs) [18],

semiconducting organic molecules and polymers [19] have been widely employed in photodetectors thus far.

As long as the application requirements allow for it, simplifying the device fabrication would contribute to realizing a more sustainable optoelectronics technology. Among various photodetector types, metal-semiconductor-metal photodetectors have the simplest architecture as they involve only a semiconductor material sandwiched between two electrodes. Nevertheless, these electrodes are often obtained using photolithography and metal evaporation or sputtering which are costly and energy-consuming.

In the literature, the colloidal quantum dot photodetectors operating in the visible regime achieved significantly high performance [20]. For example, Kim et al. reported photodetectors with detectivities $>10^{17}$ Jones and >8000 A/W between 365 to 1310 nm [21]. This performance has been achieved by integrating amorphous indium-gallium-zinc-oxide with the colloidal quantum dots and by employing expensive and energy-hungry techniques including metal evaporation, photolithography, atomic layer deposition, and radio-frequency sputtering. However, not all applications require such a high performance. For such purposes, utilizing complex, expensive, and energy-hungry techniques is a waste as an alternative, cost-effective, and more sustainable method could allow for achieving the required performance levels.

To develop such an alternative technique, here we aimed to eliminate the need for metal evaporation, sputtering or photolithography during the electrode fabrication. For this purpose, we first synthesized colloidal silver nanowires and spin-coated them on a glass substrate to form their conductive films with a sheet resistance of 95 Ω/□ while simultaneously achieving optical transparencies greater than 70%. Next, to develop an alternative method for photodetector fabrication, we carefully opened a gap in this conductive film using a surgical blade. The width of this gap was measured to be 30 μm using scanning electron microscopy. As the active layer, we employed red-emitting colloidal semiconductor CdSe/ZnS quantum dots that enable solution processing. After their synthesis, these quantum dots were simply drop-casted onto the gap opened on the conductive film. The resulting proof-of-concept device exhibited responsivities and detectivities up to 8.5 mA/W and 0.95×10^9 Jones, respectively. This metal-semiconductor-metal (MSM) photodetector demonstration shows that our method can be a sustainable, simple, and cost-effective alternative to conventional techniques.

In this thesis, in Chapter 2, we provide basic information on photodetectors. Chapter 3 is on silver nanowires, whereas Chapter 4 and 5 are about zinc oxide nanoparticles and quantum dots, respectively. In Chapter 6, we present our fabrication method and in Chapter 7 we conclude the thesis with future perspectives.

Chapter 2

Photodetectors

With the swift development of technology, optoelectronic devices including lasers, photodetectors (PDs), light-emitting diodes (LEDs), and photovoltaics (PVs) have become essential parts of everyday life. In photodetectors (PDs), photon power is converted into electrical signals such as voltage or current that are proportional to the incident optical power. PDs are among the most popular optoelectronic devices, with a wide range of uses in areas including optical communications, remote sensing, spectroscopy, imaging, etc. [22] Due to the wide range of applications, different standards are required based on the desired usage. In terms of detection wavelength, PDs can be divided into four groups: X-ray photodetectors, UV photodetectors, visible light photodetectors, and infrared photodetectors. X-ray photodetectors are utilized in industrial, security inspections, and medical imaging [23] whereas infrared photodetectors are employed in a variety of additional applications including biomedical sensing and environmental surveillance [24]. Visible photodetectors are widely employed in smartphones and cameras, including CCD (Charge-coupled Device) and CMOS (Complementary Metal Oxide Semiconductor) imaging sensors [25]. Similarly, the photodetectors used by the telecommunications industry must be very fast [26] whereas the photodetectors used for lighting applications do not require such high speeds.

In order to quantitatively evaluate the performance of PDs, a number of figures of merit have been introduced and the parameters of major importance are responsivity (R), detectivity (D*), and external quantum efficiency (EQE).

The responsivity (R) expresses the gain of the detector per unit optical power depending on the optical wavelength and defined as the ratio of the photocurrent (I_{ph}) to the incident optical power (P_o). The responsivity is calculated using Equation 1.1 [27]

$$R_\lambda = \frac{Photocurrent\ (A)}{Incident\ optical\ power\ (W)} = \frac{I_{ph}}{P_o}\ \ (A/W) \tag{2.1}$$

The detectivity (D*) that describes the smallest detectable signal that could be detectable, is calculated using Equation 1.2 where A is the effective area of the active region, R_λ is the responsivity at the wavelength λ, q is the electron charge, and I_d is the dark current [27].

$$D^* = \frac{R_\lambda \sqrt{A}}{\sqrt{2qI_d}} \qquad (cmHz^{\frac{1}{2}} W^{-1} \; or \; Jones) \tag{2.2}$$

The external quantum efficiency (EQE), the ratio of photo-generated carriers collected by photodetector to the number of incident photons, can be calculated by the Equation 1.3 where λ is the wavelength in nm, h is the Planck constant, c is the speed of light in a vacuum, and e is the elementary charge [10].

$$EQE(\lambda) = R_\lambda \frac{hc}{e\lambda} \quad (on \; a \; scale \; 0 \; to \; 1) \tag{2.3}$$

Since the requirements of applications vary widely, there are many types of photodetectors that may be suitable for specific applications [28]. These photodetector types will be explained in detail in the next section.

2.1 The p-n junction photodiodes

p-n junction photodiodes are among the most important type of photodetector. They find applications especially in the optical communication, have widely used in various applications owing to their high sensitivity, high speed, high gain, relatively small structure, low cost and long lifetime [29]. They can be fabricated from various types of materials such as silicon (Si), germanium (Ge), and indium gallium arsenide (InGaAs) [30]. Photodiodes are specifically designed to operate in reverse biased condition [10],[29],[31].

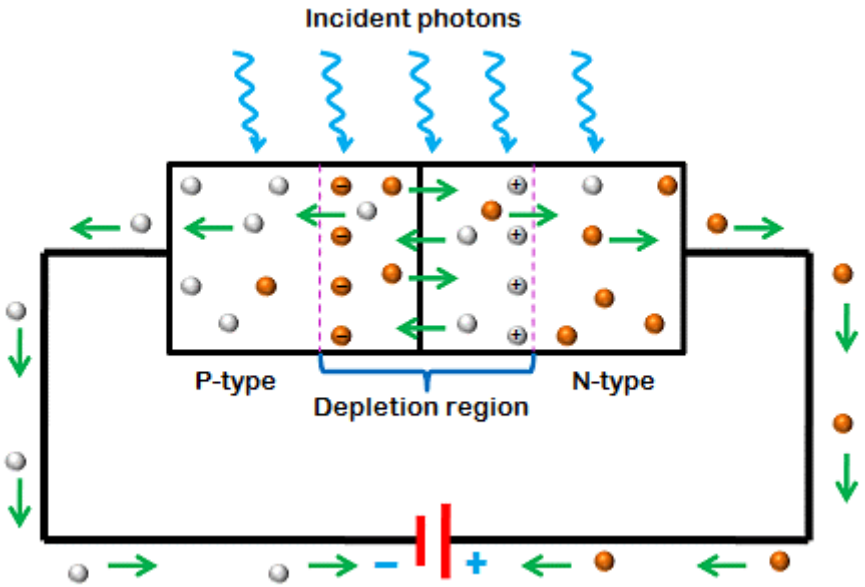

Figure 2.1 A schematic diagram of a reverse biased p-n junction photodiode [29]**.**

The photodiode creates an electron-hole pair (EHP) consisting of an electron in the conduction band (CB) and a hole in the valance band when a photon with an energy greater than the bandgap Eg strikes it (VB). The inner photoelectric effect is the name of the process that generates electron-hole pairs [32]. This photogeneration typically occurs in the depletion region. The electric field in the depletion area, which divides the EHP and causes them to drift in opposing directions, is subject to the generated EHP. Free electrons as a result move in the direction of the n-side, while holes move in the opposite direction. In the external circuit, these drifting carriers produce a current known as the photocurrent Iph [10],[29].

A photodiode operates in two different modes that are photovoltaic mode, and photoconductive mode. When the photodiodes operate without any voltage bias, this operation mode is called the photovoltaic mode (Figure 2.2 (a)) In the photovoltaic mode, no external voltage applied to the photodiode and dark current is extremely low (near zero) that reduces the noise current of the system. When a photodiode is employed in low frequency applications or low speed applications, this mode is preferred. Besides, this mode is commonly used in solar cells as it offers less variation in responsivity with temperature. However, the most significant drawback of the photovoltaic mode is the slow response speed [31].

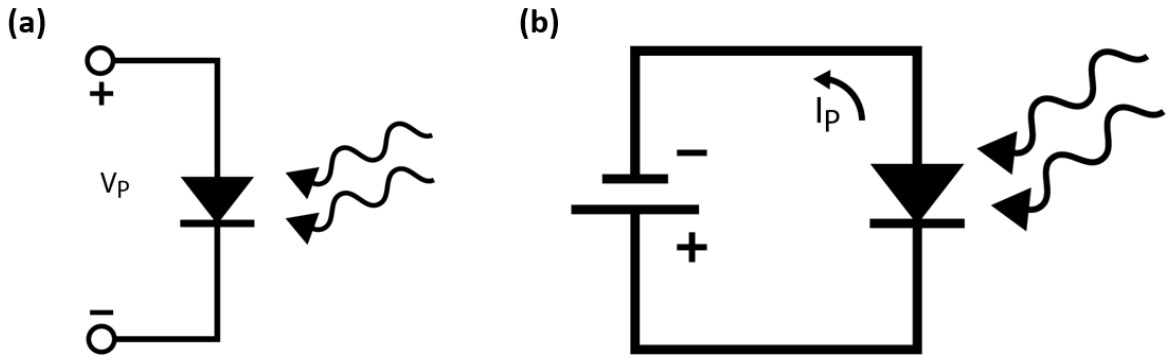

Figure 2.2 Photovoltaic mode (a) and photoconductive mode (b) of a photodiode.

In the photoconductive mode, the diode is reverse biased as shown in Figure 2.2 (b). The additional reverse bias leads to increasing the width of depletion region and reducing the junction capacitance which results in increased response speed. This reverse bias also creates the dark current without changing the photocurrent. Even though this mode is faster, the photodiodes operated in photoconductive mode have a high noise current, which can be problem for very sensitive systems [29],[31],[33].

2.2 The pin photodiodes

The p-n junction photodiodes have two significant flaws. First, the depletion layer's width, which is only a few microns at most. Accordingly, at long wavelengths where the depth of penetration exceeds the width of the depletion layer, a significant portion of photons are absorbed outside of the depletion layer where there is no electric field to separate and drift the electrons and holes, resulting in decreased quantum efficiencies. Additionally, it does not have a low enough depletion layer capacitance to enable detection at high modulation frequencies. These problems are mitigated with pin (p-intrinsic-n type) photodiode design. Although pin photodiodes are developed from the p-n junction photodiode there is a main difference, an intrinsic layer is located between the p-doped and a n-doped layers. The p-type and n-type layers are heavily doped as they are used for ohmic contacts which have a great number of charge carriers in order to carry electric current. In contrary to the p-n junction photodiode, pin photodiodes possess a wide intrinsic layer which results in reduced capacitance as the capacitance is inversely proportional with gap between p- and n-layers which makes capacitance of the pin photodiodes lower than the p-n junction photodiode. The pin photodiodes are one of the most widely used diodes in many applications including RF

switches, attenuators, and optical communication systems [34]. To fabricate the pin photodiodes, Si, Ge, and InGaAs have been widely used, similar to the p-n junction photodiodes [35].

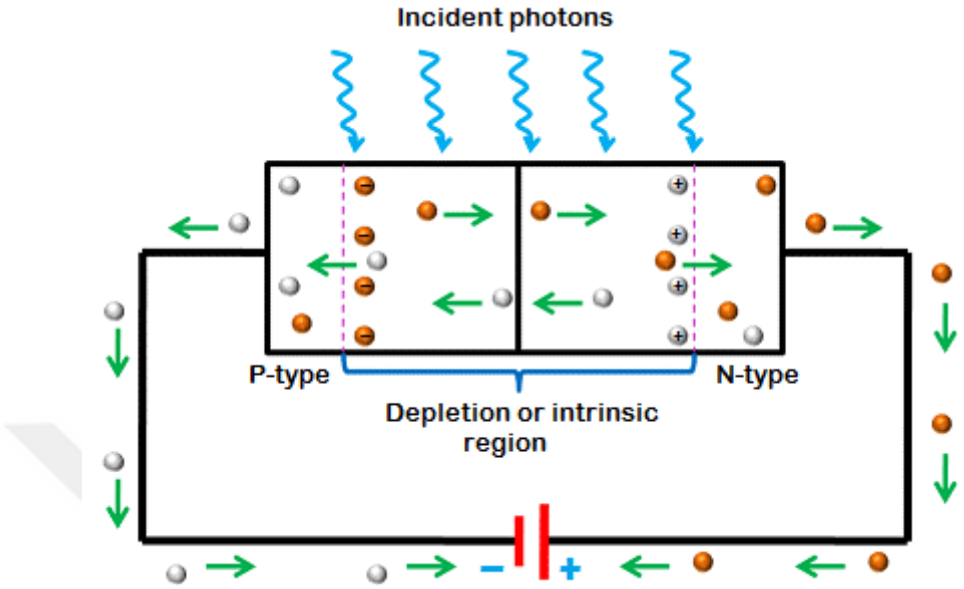

Figure 2.3 A schematic diagram of a pin photodiode [29]**.**

Similar to the p-n junction photodiodes, the pin photodiodes also operate with an applied reverse bias voltage. As it can be seen from Figure 2.3, when reverse bias is applied, the majority charge carriers in the n region and p region move away from the junction. For this reason, the depletion region starts to expand in the intrinsic layer and the width keeps expanding until it reaches (or exceeds) the width of the intrinsic layer. As a result, the majority carriers will not carry electric current under reverse bias condition since the depletion region becomes free of charge carriers. When the light with sufficient energy strikes the pin photodiode, most of the energy is absorbed by the intrinsic region due to the wide depletion width. Consequently, a large number of electron-hole pairs are generated and separated by the barrier electric field present in the depletion region. Free electrons move towards n side of the photodiode while free holes move towards p-side of the photodiode, creating a photocurrent [10], [29], [36]–[38].

2.3 Avalanche photodiodes

Avalanche photodiodes (APDs) are highly sensitive semiconductor devices that converts optical signals into electrical signals and operate at relatively high reverse bias voltage. Therefore, this allows avalanche multiplication (impact ionization) of the

charge carriers that creates an internal gain in the device to provide extra performance compared to other diodes [39].

The structure of APDs is very similar to the pin photodiodes. APDs consist two heavily doped layers (p+ layer and n+ layer) and two lightly doped layers (intrinsic (I) layer and p layer), shown in Figure 2.4 (a). In the intrinsic region, the width of the depletion layer is relatively thinner in APDs as compared to the pin photodiodes. Here, the p+ layer is connected to the negative terminal of the battery while n+ layer is connected to the positive terminal of the battery.

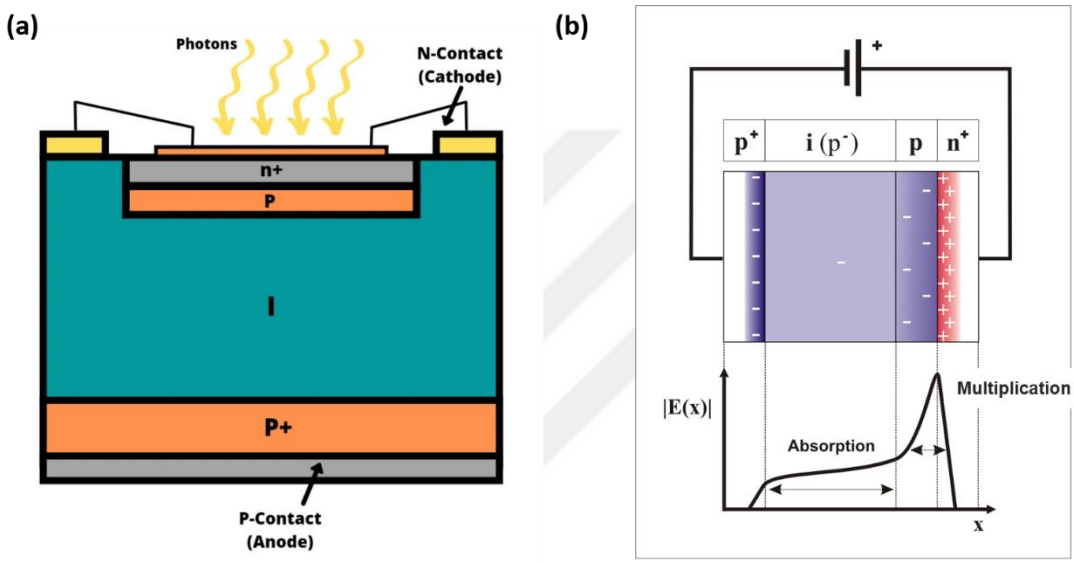

Figure 2.4 Avalanche photodiode structure (a) and its circuit diagram (b) [40]**.**

Avalanche breakdown takes place once the APD exposed to relatively high reverse bias voltage. This voltage boosts the electric filed across the depletion layer. As it can be seen from Figure 2.4 (b), when an incident light enters in p+ layer, it becomes absorbed in the immensely resistive p layer. At this point, electron-hole pairs are generated. Charge carriers are dragged with their saturation velocity towards the pn+ layer where a high electric field exists. When the velocity reaches its maximum value, carriers collide through other atoms and generate new electron-hole pairs. As a result of large number of generated electron-hole pairs, high photocurrent is obtained.

APDs are widely used in optical communications [41] owing to their internal gain and high speed [10]. They are also employed for high frequency modulation and high sensitivity applications including laser scanners, spectrometers, and encoders [42]. As mentioned before, structure of APDs is very similar to pin photodiodes. However,

APDs provides extra performance compared to other diodes. Table 2.1 shows a simplified chart comparing avalanche photodiodes and pin photodiodes.

Table 2.1 Comparison of APDs and pin photodiodes [40]

Parameters	**Avalanche Photodiode**	**PIN Photodiode**
Layers	Four layers (p+/I/p/n+)	Three layers (p+/I/n+)
Response time	Very high	Very low
Sensitivity	High	Low
Internal gain	≤200 dB	Insignificant
Output current	Low value of current	Carrier multiplication results in amplified current
Noise	Higher owing to charge multiplication	Relatively lower than APD
Reverse bias voltage	Extremely high	Low
Temperature stability	Great	Poor

2.4 Schottky junction photodiodes

In the previous sections, avalanche photodiodes and pin photodiodes discussed which are both p-n junction devices. Unlike these diodes, the Schottky junction (SJ) photodiodes employ a metal-semiconductor (n-type) junction in order to separate and collect the photogenerated charge carriers [43]. Generally, these junctions are deposited onto substrate by metal evaporation in vacuum. SJ photodiodes have been widely used in optoelectronic applications, especially in CCDs (charge coupled device) [44], on account of their numerous advantages.

The depletion layer, also known as the space charge layer (SCL), being close to the metal contact is a significant benefit of the SJ photodiode. In an SJ photodiode, the SCL absorbs the short-wavelength light that was previously absorbed in the neutral zone close to the electrode in a p-n or pin photodiode. Therefore, whereas minority carriers in p-n and pin photodiodes have to diffuse to the SCL, photogenerated EHPs can be instantaneously separated, drifted, and collected. In fact, a significant portion of EHPs in p-n and pin photodiodes diffuse to the surface and disappear via recombination.

SJ photodiodes also have the benefit of being far faster than p-n or pin photodiodes. The majority of carriers are electrons, which are injected. Therefore, they are not limited by the minority carrier recombination time. Furthermore, they have a

bandwidth of up to hundreds of gigahertz [43]. SJ photodiodes are utilized in pairs in the so-called interdigitated electrode structure, which is produced on the same semiconductor surface, in high-speed applications, optical communication, or optical measuring technology, as shown in Figure 2.5 (a) and (b) (b). Between the electrodes, a semiconductor absorbs the light [10].

Because of all these advantages of Schottky diodes in addition to the simplest architecture as they involve only a semiconductor material sandwiched between two electrodes, we utilized this structure in order to fabricate colloidal quantum dot photodetectors. The fabrication technique will be comprehensively explained in the related section.

As seen in Figure 2.5(a), the anode and cathode of the battery are connected to two digital electrodes, A and B. One of the Schottky junctions will always be reverse biased because they are connected end to end but in opposing directions. The energy band diagram is symmetric without any applied bias, as seen in Figure 2.5(c). The depletion layers for A and B are referred to as SCL_1 and SCL_2, respectively. A and B junctions have built-in voltages of V_{o1} and V_{o2}, respectively. When an electron-hole pair is photogenerated in the semiconductor, they cannot drift and become collected as they can in a single SJ device. As indicated in the Figure 2.5 (c), they are inserted between two potential barriers. In contrast, in a single Schottky junction, the photogenerated EHPs within the SCL can be collected as they become separated and drifted.

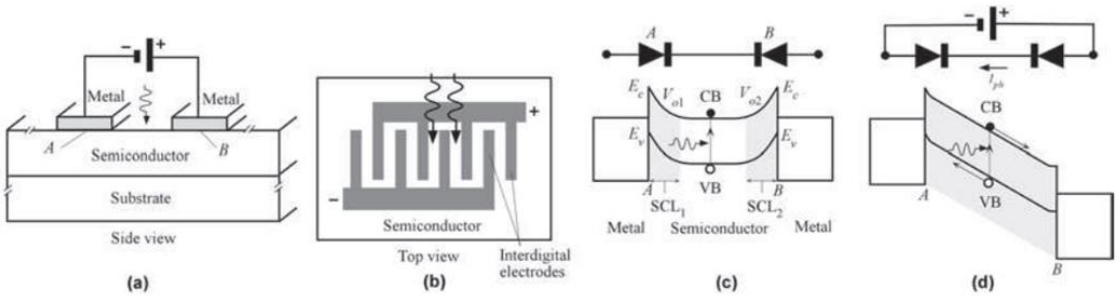

Figure 2.5 Schematics of a Schottky junction photodiode. (a) The semiconductor crystal (which is formed on a suitable substrate) has metal electrodes on its surface. (b) The electrodes are arranged to be interdigital and located on the crystal's surface. (c) As shown for A and B, two adjacent Schottky junctions are connected end to end but in different directions. Without any bias, the energy band diagram is symmetrical. The SCL_1 and SCL_2 at A and B are shown by the gray areas. (d) When the bias is high enough, the SCL_1 from A expands and meets that

from B, depleting the entire semiconductor between the electrodes. This area has a strong field, which causes the photogenerated EHPs to separate and drift, creating a photocurrent.

Due to A's reverse bias and B's forward bias, when a voltage is applied, V_{o1} will increase and V_{o2} will decrease (Figure 2.5(d)). The dark current is incredibly small because A is reverse biased. The right side of the band (B) must be bent down by eV_r to account for the applied voltage, as seen in Figure 2.5 (d), since by the time the electron from A reaches B, its potential energy must have decreased by eV_r. A further increase in voltage will result in a greater voltage drop on SCL_1 than on SCL_2 since the applied bias expands SCL_1 and shrinks SCL_2 in the semiconductor. When the voltage is high enough, the reverse bias on A extends SCL_1 to the point that SCL_2 breaks down as a result, depleting the entire semiconductor between the electrodes. The reach-through voltage is the name given to the corresponding bias voltage. An electron and a hole produced by photogeneration can roll down their respective energy hills since there is now a strong field in this depletion zone.

2.5 Colloidal quantum dot photodiodes

To date, crystalline inorganic semiconductors like silicon and III-V and II-VI compounds have dominated photodetection and sensing technologies [45]. However, it is expensive, time-consuming, and energy-intensive to produce these materials and devices [46].

To meet numerous requirements in different applications as well as to overcome the high-cost problem, there have been substantial demand on the new detection tools that can be compatible with diverse substrates. Due to their excellent qualities, such as size tunability, solution processability, cheap production cost, and high absorption coefficient, colloidal quantum dots (CQDs), an emerging class of material for optoelectronic devices, have attracted interest [47]. CQDs have thus been widely used in a variety of applications, particularly in optoelectronic devices like photodetectors.

The following substances could be used to create CQDs: CdS, CdSe, CdTe, ZnS, ZnSe, ZnTe, HgTe, PbSe, PbS, and InP. However, a high photoluminescence quantum efficiency—defined as the number of photons emitted per absorbed photon—is typically not achieved by using simply core. A core/shell material system is preferred to boost the emission capabilities of CQDs. In this setup, the core is surrounded by extra material

with a larger band gap. Lattice mismatch is reduced through careful material selection, which raises quantum efficiency[48]. As a result, more effective CQDs may be created. CdSe/CdS, CdSe/CdS/ZnS, CdSe/ZnS, PbSe/PbS, CdTe/CdSe, CdSe/ZnTe, and InP/ZnS are common material options [49].

PbS colloidal quantum dots, in particular in colloidal quantum dot photodiodes, have gained interest among these materials in optoelectronic devices. The full SWIR and visible spectrum from 1800 to 700 nm can be covered by adjusting the dot size from 10 to 2 nm in diameter (Figure 2.6). PbS colloidal quantum dot photodiodes can address spectral windows of interest in a variety of crucial applications, including visible video and photography, near-infrared biomedical imaging, SWIR night vision, and all of the mentioned for spectroscopy and broadband applications [50].

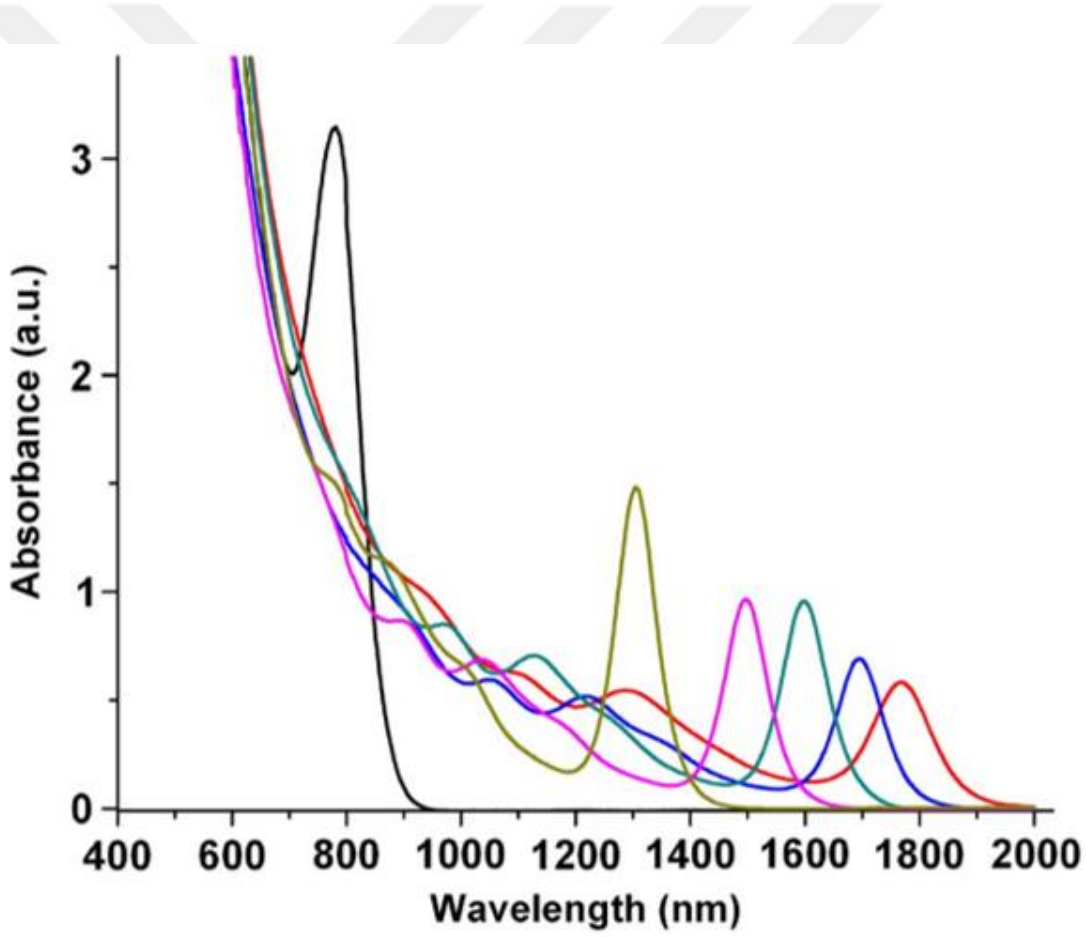

Figure 2.6 Tunability of quantum size effects in the absorption spectra of PbS colloidal quantum dots. Quantum dot sizes vary in diameter from 10 nm (red) to 3 nm (black) [50]**.**

Colloidal quantum dot photodiodes mainly consist of an electron transfer layer (ETL), a hole transfer layer and photoactive layer, as shown in Figure 2.7 (a). Photogenerated carriers in the CQD layer are separated by built-in electric field in the device and similar to other photodiode types, are operated with applied reverse bias voltage (Figure 2.7 (b)). This type of photodiodes typically has no gain however high gain can be achieved with photodiodes based on trap-induced charge tunneling injection [10].

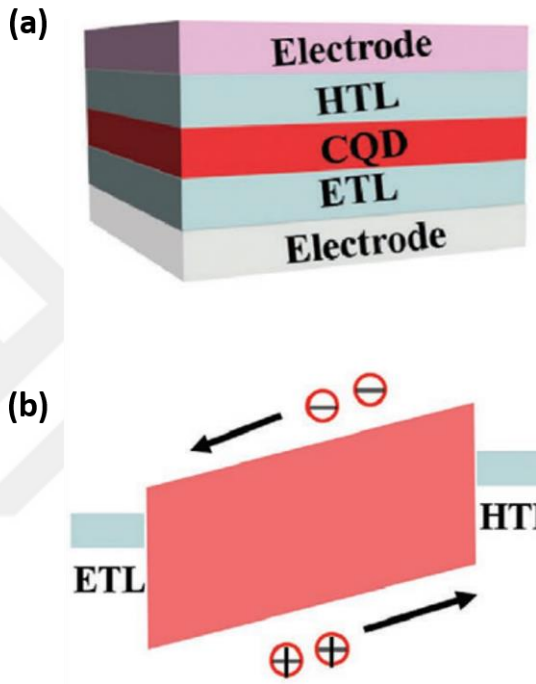

Figure 2.7 Schematic diagrams of colloidal quantum dot photodiodes device architecture (a) and their energy band diagram (b) [10]**.**

Colloidal quantum dots are typically deposited between electrodes to create these types of photodiodes, also known as metal-CQD-metal photodiodes. Broad band photodetection from the deep ultraviolet (DUV) to mid-infrared (MIR) range, ultrahigh photoresponsivity and detectivity, long-term stability, and fast rise and fall times have all been accomplished by CQD-based photodiodes to date. For instance, a PbS CQD-based CQD photodiode with high sensitivity and a specific detectivity value up to $3.2x10^{11}$ Jones at 1125 nm was demonstrated by Xu et al. [51]. Additionally, Tang et al. demonstrated a CQD photodiode based on modified PbS CQDs that under 1550 nm illumination demonstrated a responsivity (R) of 5.15 A/W, a response time of 110 s, and a specific detectivity of $1.96x10^{10}$ Jones [52].

Chapter 3

Silver nanowires (Ag NW)

3.1 Silver nanowires as transparent electrodes

As long as the application requirements allow for it, simplifying the device fabrication would contribute to realizing a more sustainable optoelectronics technology. Among various photodetector types, metal-semiconductor-metal photodetectors have the simplest architecture as they involve only a semiconductor material sandwiched between two electrodes. Nevertheless, these electrodes are often obtained using photolithography and metal evaporation or sputtering which are costly and energy-consuming.

Developing a sustainable photodetector fabrication technology necessities elimination of traditional fabrication tools. For this purpose, we focus on using silver nanowires (Ag NW) as electrodes because of their excellent electrical conductivity, optical transparency, high flexibility and strong stretchability. Ag NW, which are 1-dimensional (1-D) silver nanostructures with diameters between 10 and 200 nm and lengths between 5 and 100 μm, have attracted a great attention for their use as transparent electrodes [53], in wearable sensors [54], solar cells [55], and gas sensors [56],[57].

Over the past fifty years, indium tin oxide (ITO) has been utilized extensively as a transparent electrode in numerous applications, particularly in optoelectronics. However, its brittle structure, in addition to scarcity and high cost, prevents it from being used further in many fields. It has been discovered that there are various transparent conductive materials, each with specific features, including graphene, carbon nanotubes, and metal nanowires, thanks to advancements in nanomaterials. [58].

Table 3.1 compares the performances of these substitute materials, including electrical conductivity, light transmission, flexibility, manufacturing cost, and material

cost. As listed in Table 3.1, only silver nanowires (Ag NW) have shown superior optoelectronic performance over ITO among these materials that serve as alternatives. [59].

Compared to other materials, the advantages of Ag NW are as follows:

1. One can obtain highly transparent conductive films by thin coating of silver nanowires

2. The silver nanowire films are flexible and stretchable. It is possible to fabricate flexible electronic devices.

3. The silver nanowire synthesis comprises fully solution-processing which can be scaled-up for lower cost [60]. Because of these outstanding properties, we have decided to use Ag NW as a transparent conductive electrode.

Table 3.1 Performance comparison of Ag NW and others transparent materials.

	Ag NW	ITO	Graphene	Carbon nanotubes
Conductivity	✓	✓	✓	
Light transmission	✓	✓	✓	✓
Flexibility	✓		✓	✓
Manufacturing cost	✓	✓		✓
Material cost	✓	✓		

3.2 Synthesis Techniques

Researchers have proposed several methods in order to prepare silver nanowires over the years. The main purpose has been obtaining uniform Ag NW with high yield since the uniformity and crystal quality of the nanowires affect the electronic and optical features of the Ag NW films. Initially, Ag NW were mostly prepared via electrochemical methods. However, this technique caused environmental pollution as well as the synthesized Ag NW were not uniform and had low yield. As an alternative, the template method has been employed for Ag NW synthesis, but high-cost of the template fabrication and low yields in addition to irregular morphologies restrict the further developments using this approach. The wet chemical method and the polyol

method have been more convenient for preparing Ag NW. Among all of these methods the polyol method turned out to be more advantageous as it offers a better dimension control, low production cost, higher yields, and more uniformity. Table 3. compares the diameter and length of Ag NW synthesized using different techniques [61],[57]. In this thesis work, we employed polyol method that offers reasonable dimensions suitable for electronic conductivity and optical transparency while keeping the production costs manageable.

Table 3.2 Typical dimension of Ag NW obtained by different synthesis methods.

Synthesis Method	Diameter (nm)	Length (µm)	Reference
Electrochemical method	4	50-300	[62]
Template method	5-200	>50	[63]
Wet chemical method	20-40	>1	[64]
Polyol method	30-40	>50	[65]

3.2.1 Synthesis of Ag NW

Chemicals and Materials

Polyvinylpyrrolidone (PVP, Mw ≈ 40000, powder), silver nitrate (AgNO3, 99.0%), sodium chloride (NaCl, 99.5%), potassium bromide (KBr, 99.0%), ethylene glycol (EG, 99.0%). All chemicals and reagents were purchased from Sigma-Aldrich unless otherwise stated and used without further purification.

Ag NW were prepared using a modified version of the polyol process developed by Kim et al. [66]. First, 50 mL of EG and 1.6 g of PVP were added in a two-necked flat-bottom flask and stirred at 450 rpm with a magnetic stirrer until the PVP was completely dissolved. The mixture was then heated to 170 °C, and 0.05 g of NaCl, 0.025 g of KBr, and 0.7 g of AgNO3 were added while the mixture was still being stirred. Next, the solution was kept at 170 °C for 3 h to allow the Ag nanowire growth reaction to take place and then was cooled down to room temperature by moving the flask into water bath. In order to get rid of the impurities, the nanowire solution was centrifuged with methanol and acetone (3:1) twice at 5000 rpm for 10 min. The collected Ag NW were finally dispersed in ethanol.

After synthesis, we examined the structure of Ag NW by using scanning electron microscopy (SEM) and analyzed the dimension of nanowires. Figure 3.1 (a-b) shows that SEM images of Ag NW with a length and diameter histogram. As it can be clearly seen in Figure 3.1 (c-d), the obtained nanowires appear to be straight wires with an average diameter of 43 nm and average length up to over 7 µm.

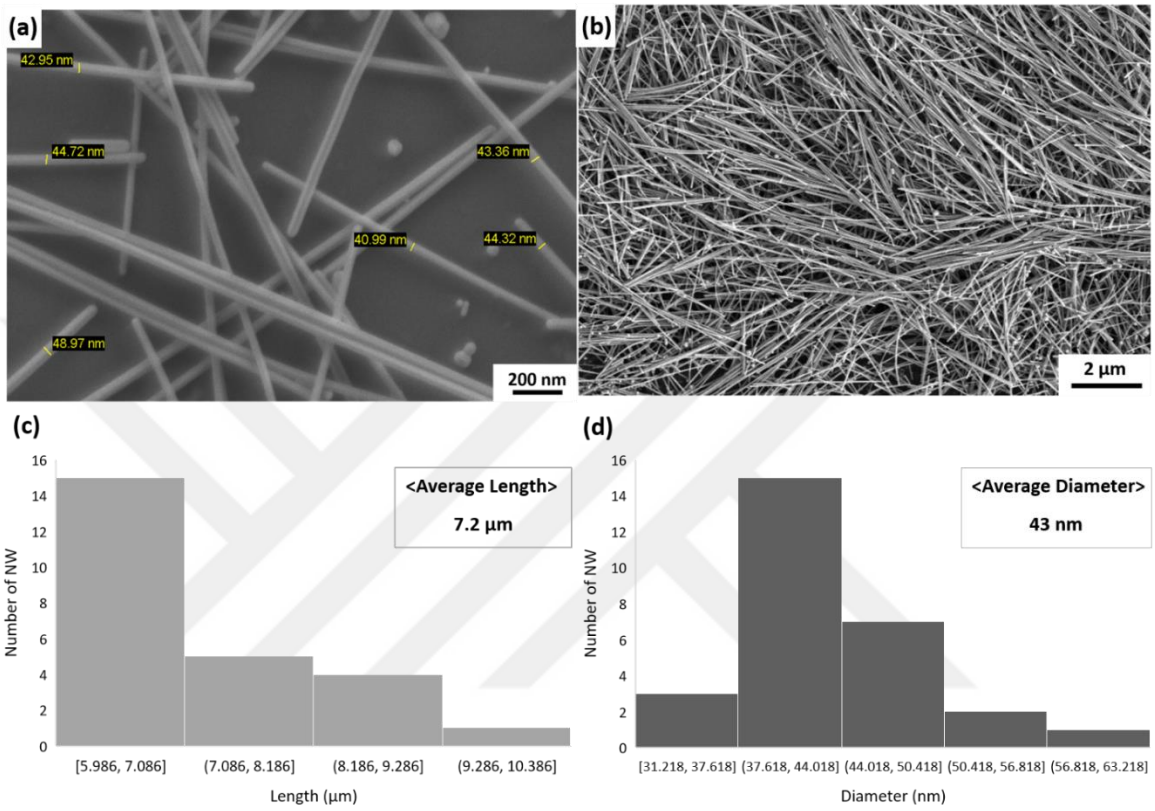

Figure 3.1 (a)-(b) SEM images of synthesized Ag NW networks on a glass substrate. The Ag NW length (c) and diameter histogram.

3.3 Electrical properties of Ag NW thin films

Electrical characteristics of Ag NW are very significant since they utilize as a transparent conductive electrode for an optoelectronic device. In order to get information on the electrical conductivity, one can utilize sheet resistance of materials that indicates the resistance of thin films. The unit of the sheet resistance is ohm per square (Ω/□) [67]. For measuring the sheet resistance, the four-probe method which is performed using a four-point probe is used. The main reason of using the four-probe method is eliminating the effect of contact resistance [64]. Equation 3.1 below can be used to calculate the sheet resistance [65]:

$$R_s = \frac{\pi}{\ln(2)} \frac{\Delta V}{I} = 4.53236 \frac{\Delta V}{I} \quad (3.1)$$

where the ΔV and I stand for the supplied voltage and the current flowing through the film, respectively.

The sheet resistance of Ag NW network is related to the characteristics of single Ag NW. We used the four-probe approach to measure the sheet resistance of the films as a function of the number of metal nanowire spin-coating cycles in order to reveal these basic characteristics of nanowire thin films. To analyze the effect of the number of Ag NW layers on the conductivity, we spin-coated the Ag NW solution various times on a glass substrate. As shown in Figure 3.2, the sheet resistance of Ag NW films decreases with increasing number of spin-coating cycles starting from MΩ/□ levels for two layers of coating to ~180 Ω/□ for ten coating cycles.

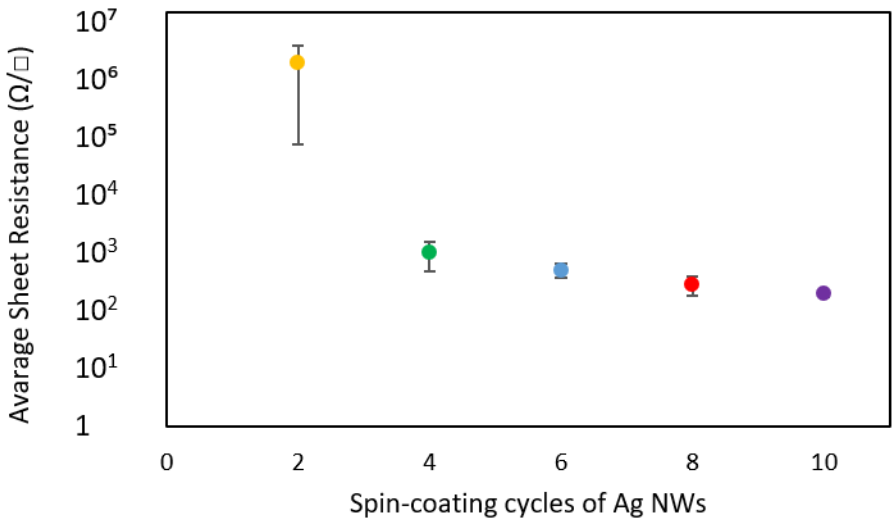

Figure 3.2 Average sheet resistance of Ag NW films as a function of spin-coating cycles. The level shown by each marker indicates the average sheet resistance of five measurements on the film whereas the error bars stand for the standard deviation of those measurements.

To improve the Ag NW adhesion on substrate and enhance conductivity, we spin coated zinc oxide nanoparticles (ZnO NP) on Ag NW network, that will be explained in the following section.

3.4 Optical properties of Ag NW thin films

Ag NW show high optical transparency as well as high electrical conductivity in the visible region that makes them attractive for various applications including transparent electrodes [43], wearable sensors [45], solar cells [46], and gas sensors [47]. The optical transparency of Ag NW films strongly depends on size and shape of Ag NW. It is well known that the frequencies of particular localized surface plasmon resonance bands depend on the size and shape of Ag NW [53]. Based on this principle, one can obtain information on the morphology of Ag NW through characterization of their optical properties. To measure the optical properties of materials, the UV spectroscopy is frequently employed. Figure 3.3 presents the synthesized absorption spectrum of Ag NW colloidal solution. The smaller absorption peak at 350 nm was attributed to the longitudinal mode or the out-of-plane quadrupole mode and the strong peak at 380 nm was ascribed to plasmon resonance peaks of silver due to transverse mode of nanowires [66], [67].

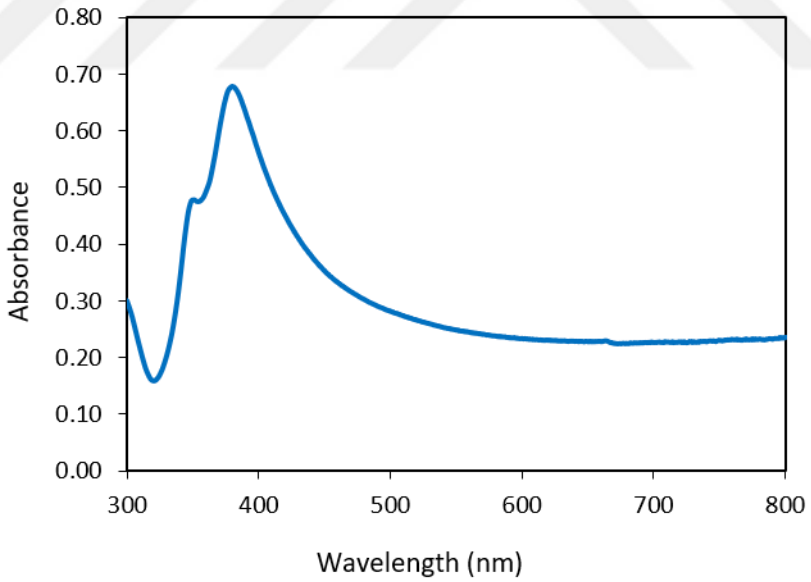

Figure 3.3 UV-visible absorption spectra of synthesized Ag NW colloidal solution.

The applications of flexible transparent electrodes in optoelectronic devices are directly influenced by optical transparency, one of the fundamental factors for evaluating Ag NW networks. One can generally evaluate optical performance by transmittance which is measured by using UV-visible spectroscopy. The optical transparency heavily depends on size and shape of Ag NW. Once the density of Ag NW increases, the light transmittance will decrease [57]. In order to investigate the effect of

the number of Ag NW layers on the transparency, we spin-coated the Ag NW solution various times. As shown in Figure 3.4, the transmittance of the Ag NW films decreases with increasing number of spin-coating cycles. After two spin-coating cycles the transmittance was found to be >90%. It remains still ~70% in the visible regime at the end of ten spin-coating cycles whereas the commercially available indium tin oxide films possess transmittances of ~90% in the visible regime [68]. These results show that our Ag NW can exhibit high transparency and low sheet resistance, meaning these materials suitable for optoelectronic devices although ITO outperform the Ag NW.

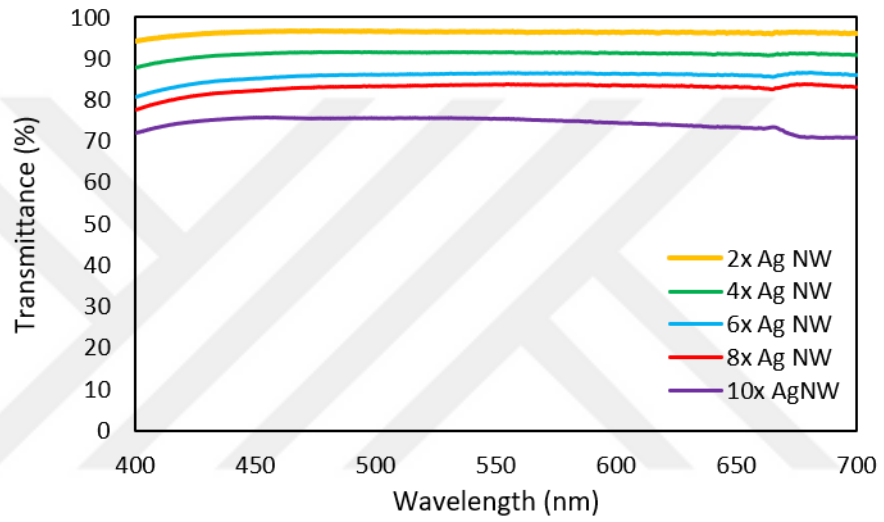

Figure 3.4. Transmittance spectra of Ag NW films obtained by spin-coating of Ag NW at various numbers.

Chapter 4

Zinc oxide nanoparticles (ZnO NP)

4.1 Zinc oxide nanoparticles as additives for transparent and conductive Ag NW film

Zinc oxide, an n-type semiconductor, is an inorganic chemical compound that is frequently employed in daily life. Among the metal oxide semiconductors, zinc oxide has been intensely studied because of its wide band gap around 3.37 eV allowing for high optical transparency [69]. In addition, the oxygen vacancies on ZnO creates an n-type material with high electron density [70]. This high electron density enables their use in light emitting devices as electron transport layer. Due to these unique properties, ZnO is a promising material for optoelectronic applications [71]. Zinc oxide nanoparticles have emerged in recent years as a result of the rapid growth of nanotechnology. [72]. Zinc oxide nanoparticles (ZnO NP) with diameters below 100 nm has been widely used in many areas including cosmetics, food additives, photoelectricity and rubber industry owing to their excellent UV absorption, higher chemical activity, corrosion resistance, photocatalysis, shielding ability to ultraviolet rays [73]–[77].

4.2 Synthesis techniques

Due to its outstanding characteristics and numerous prospective uses, particularly in optoelectronics, the synthesis of ZnO NP has attracted a lot of interest. Physical vapor synthesis (PVS) and mechanochemical processing (MCP) are the two main methods used to synthesize ZnO NP [78]. Precipitation, thermal decomposition,

hydrothermal synthesis, laser ablation, microwave-assisted combustion method, sol-gel method, ultrasound, anodization, coprecipitation, electrochemical depositions, and electrophoretic deposition are other methods for synthesizing ZnO NP in addition to these [79],[80]. Among these techniques, sol-gel method is widely used since it is the simplest method and capable of controlling particle size and morphology through systematic monitoring of reaction parameters [81]. In this thesis, we synthesized colloidal ZnO NP by using the sol-gel method.

4.2.1 Synthesis of ZnO NP and integration with Ag NW films

Chemicals and Materials

Zinc acetate dihydrate ($ZnAc.2H_2O$, 99.999%), dimethyl sulfoxide (DMSO, Merck), tetramethylammonium hydroxide pentahydrate (TMAH, ≥97%, Sigma-Aldrich), ethanol absolute (≥99.9%, Isolab), acetone (EMSURE, Merck), n-hexane (≥96%, Merck). All chemicals and reagents were purchased from Sigma-Aldrich unless otherwise stated and used without further purification.

The synthesis of ZnO nanoparticles was carried out with some modifications to the recipe adapted from Jin et al. [82]. For the synthesis, two different solutions were prepared. For the first of these, 0.6585 g of zinc acetate dihydrate was dissolved in 30 mL of dimethyl sulfoxide (DMSO) and the solution was left stirring. Secondly, a tetramethylammonium hydroxide pentahydrate (TMAH) solution in ethanol was prepared (0.5 M, 10 mL). While mixing the zinc acetate dihydrate solution with a magnetic stirrer, the TMAH solution was dropped into it at a rate of 8 mL/min. The solutions were then allowed to react for 1 hour at ambient conditions without interrupting the mixing process. After the reaction, the obtained solution was divided equally into 3 falcon tubes of 50 mL and filled with acetone [83]. They were centrifuged at 5000 rpm for 5 minutes. Right after this process ended, the supernatant was poured out while the precipitate was kept. Subsequently, 1 mL of ethanol was added to each falcon tube and sonicated for 10 minutes in a cold sonicator. Then, 24 mL of acetone and then 25 mL of hexane were added to each 1 ml solution and centrifuged at 5000 rpm for 10 min. Similarly, after the centrifugation process, the liquid part was drained from the falcon and 1.5 mL of ethanol was added. Finally, they were sonicated in a cooled sonicator for 15 minutes before further use.

After synthesis, we spin-coated ZnO NP on to Ag NW network and analyzed the morphology of this thin film by SEM shown in Figure 4.1. The SEM image demonstrates that uniform formation of spherical ZnO NP.

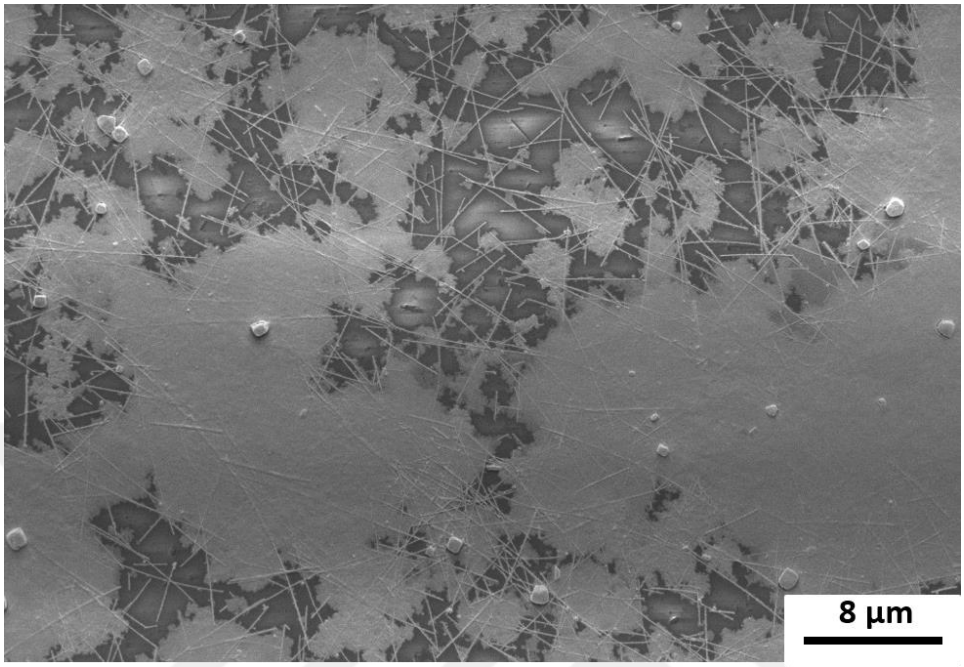

Figure 4.1 SEM image of the synthesized ZnO NP spin-coated on Ag NW networks.

4.3 Optical properties of ZnO NP

ZnO NP display high optical transparency in the visible regime since they have a wide band gap of 3.37 eV. To examine the optical properties of ZnO NP, we employed UV-visible absorption spectrum. Figure 4.2 represents the UV-VIS absorbance spectrum of ZnO NP. It shows strong absorption band about 350 nm [74].

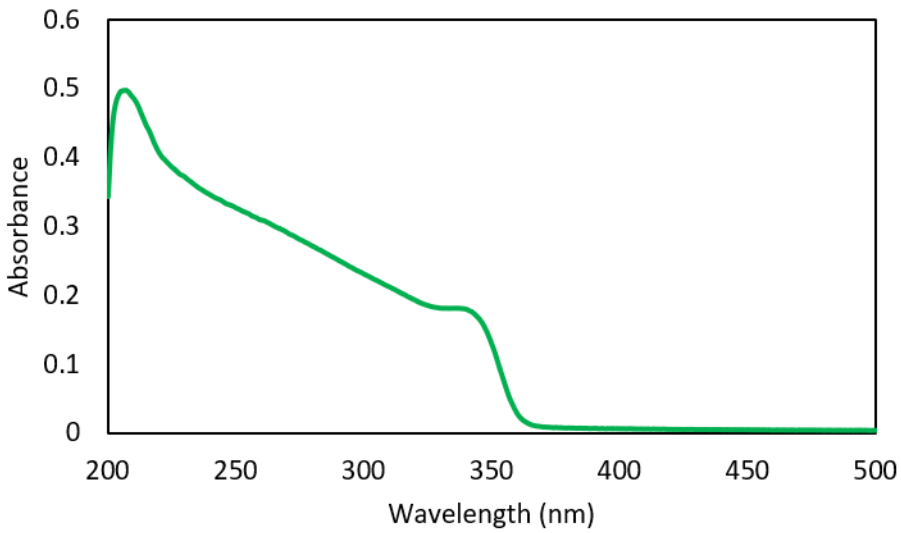

Figure 4.2 UV-visible absorption spectra of the ZnO NP dispersion.

Furthermore, we investigate the effect of ZnO NP on optical transparency through coating them on to Ag NW network. As presented in Figure 4.3, the transmittance of the Ag NW-ZnO films decreases with increasing number of spin-coating cycles but its transmittance value remains still higher than 70% for the spectral range in the visible region at the end of ten spin-coating cycles similar to only Ag NW coating.

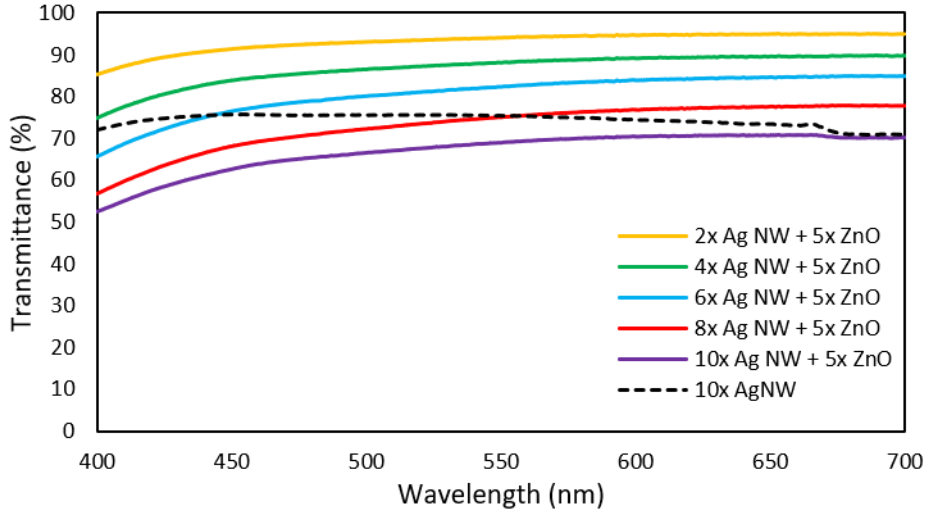

Figure 4.3 Transmittance spectra of Ag NW-ZnO films obtained by spin-coating Ag NW at various numbers.

4.4 Electrical properties of ZnO NP

As mentioned in the previous section, by only spin coating Ag NW on a glass substrate, we formed a highly conductive transparent film whose sheet resistance becomes ~180 Ω/□ as measured by the four-probe method. However, there were some problems with utilizing only Ag NW to obtain conductive films. One of these problems was that the adhesion of Ag NW on glass substrate was very weak. To overcome this problem, after a long literature research, we found that Tang et al. recommended to using ZnO to obtain highly conductive and transparent electrodes as well as improve the Ag NW adhesion on substrate [84]. In addition to achieving a high transparency, obtaining conductive films is also an important motivation of this work. According to Kashkool et al. [85], the lowest sheet resistance of ZnO films is at 200 ºC. On the other hand, Choo et al. [86] demonstrated that after 150 ºC the sheet resistance of Ag NW films decreases. Considering the results of these earlier works, we fixed the annealing temperature at 150 ºC to obtain the lowest sheet resistance. Subsequently, we tested the sheet resistance of the films as a function of number of metal nanowire spin-coating cycles. As shown in Figure 4.4, the sheet resistance of Ag NW-ZnO films decreases with increasing number of spin-coating cycles starting from kΩ/□ levels after two layers of coating to ~95 Ω/□ after ten coating cycles.

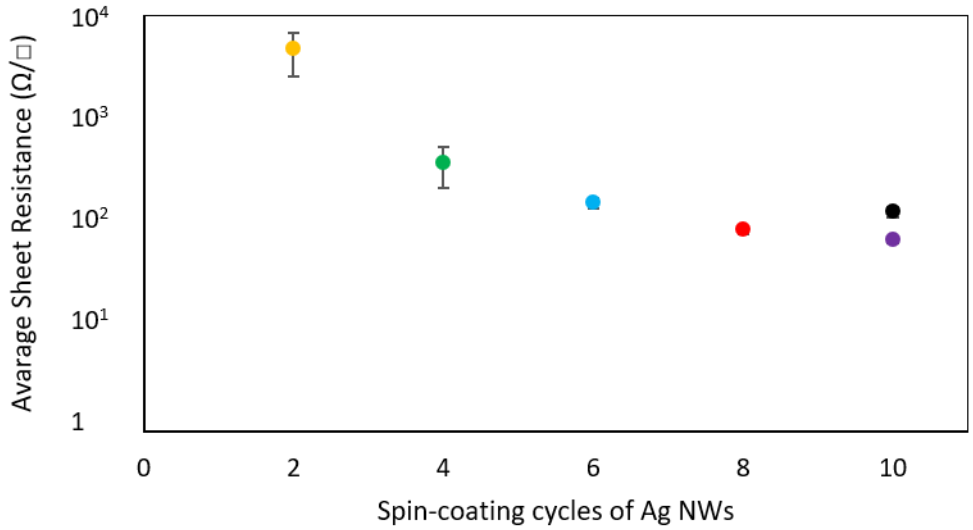

Figure 4.4 Average sheet resistance of Ag NW films as a function of spin-coating cycles. The level shown by each marker indicates the average sheet resistance of five measurements on the film whereas the error bars stand for the standard deviation of those measurements. The black marker shows the sheet resistance of the sample that is not treated with ZnO NPs.

Chapter 5

Colloidal Quantum Dots (CQDs)

5.1 Colloidal quantum dots for photodetectors

Commercialized visible photodetectors are generally based on traditional crystalline semiconducting materials such as silicon, germanium, gallium arsenide, etc. However, their growth requires costly, high temperature methods. As an alternative to these materials, colloidal quantum dots (CQDs) emerged starting from early 90s.

Colloidal quantum dots which are quantum-confined semiconductor nanocrystals with diameters below 20 nm have been frequently utilized in photodetector applications and they have appealed attention in view of their solution-processability, low-cost manufacturing, high absorption coefficient, and wide range bandgap tunability [87]. Besides, they have surface ligands that enable their dispersion in common solvents [88]. Their solution-process ability and easy manufacturing allowed for their utilization in various optoelectronic devices such as light-emitting diodes (LED) [89], solar cells [90], photodetectors [91], and lasers [45],[92].

When a photon with enough energy (equal or greater than the bandgap) strikes a semiconductor material, it can promote an electron from the valence band to the conduction band, generating an electron-hole pair. This process is referred to as "excitation process". Electrons can release extra energy into heat when they are stimulated to the conduction band, which brings their energy down to a level close to the band edge. the procedure known as "relaxation process". When the excited electron and hole recombine, the gained energy will be released as a new photon. This photon radiates the energy of the bandgap because it is emitted from the band edge of the conduction band to the band edge of the valence band (Figure 5.1) [94].

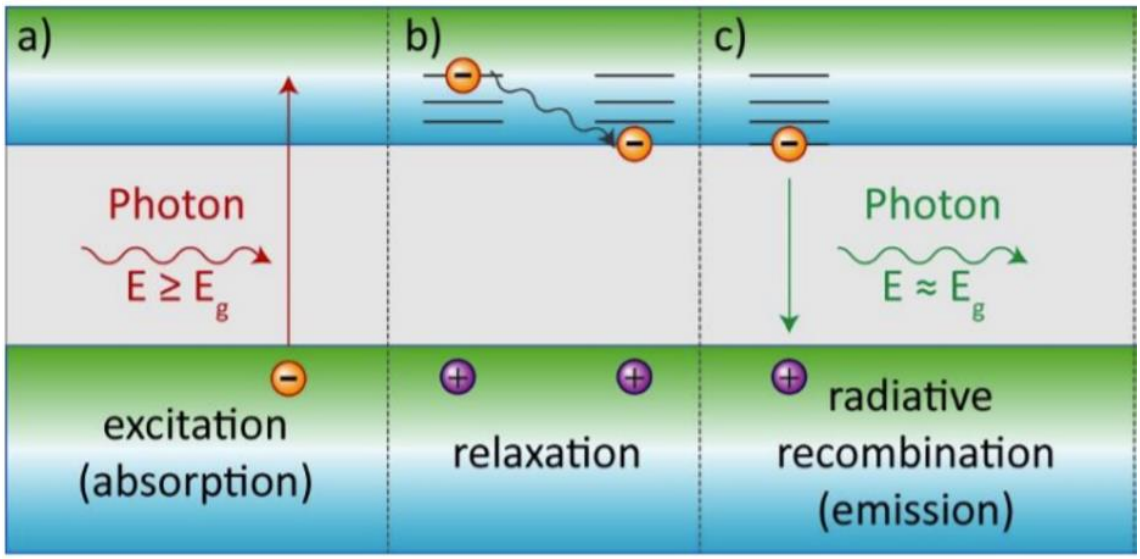

Figure 5.1 Interaction of photons with semiconductors. Three processes- (a) photon absorption, (b) electron relaxation, and (c) radiative recombination—lead to the emission of photons. [95]**.**

The quantum confinement effect gives colloidal quantum dots their distinctive optical features, and the energy of the bandgap determines the color of the light that is emitted. Different sized CQDs emit various colored light.

In a strong quantum confinement, the bandgap increases once the CQDs is smaller than exciton Bohr radius due to the discrete energy levels. The exciton Bohr radius (r_B) of a bulk semiconductor can be calculated using Equation 5.1 where ħ is the reduced Plank's constant, e is the electron charge, ε is the permittivity, m_e is the electron effective mass, and m_h is the hole effective mass [96].

$$r_B = \frac{\hbar^2 \varepsilon}{e^2}\left(\frac{1}{m_e} + \frac{1}{m_h}\right) \tag{5.1}$$

When r_B is calculated for a typical semiconductor used for CQDs, it is found about 5 nm. According to this, the particle remains in the weak confinement regime since radius of a crystalline, the size of a typical CQDs is ~10 nm, greater than the r_B [97]. As a result, the energy of exciton can be expressed by Equation 5.2 where E_g is the bulk bandgap energy, n, m, and l are the quantum numbers, R_y^* is the exciton Rydberg energy, M is the mass, a is the size of the particle, and χ_{ml} is the roots of the Bessel function [96].

$$E_{nml} = E_g - \frac{R_y^*}{n^2} + \frac{h^2 \chi_{ml}^2}{2Ma^2} \tag{5.2}$$

Equation 5.2 demonstrates that when particle size drops, the size-dependent transition energies increase. The emission and absorption spectrum of CQDs provide evidence of this. Depending on the material from which the CQDs are constructed and the size of the CQDs, the CQDs absorb across a wide range and emit light over a narrow range that can be tuned [97]. A noticeable blue shift in the emission spectra of the semiconductor material is seen when CQD size decreases (Figure 5.2 (a)). The absorption features exhibit a size-dependent behavior, just like the emission. The absorption stars at higher photon energy or shorter wavelengths are produced when the size of the CQDs decreases (Figure 5.2 (b)) [49].

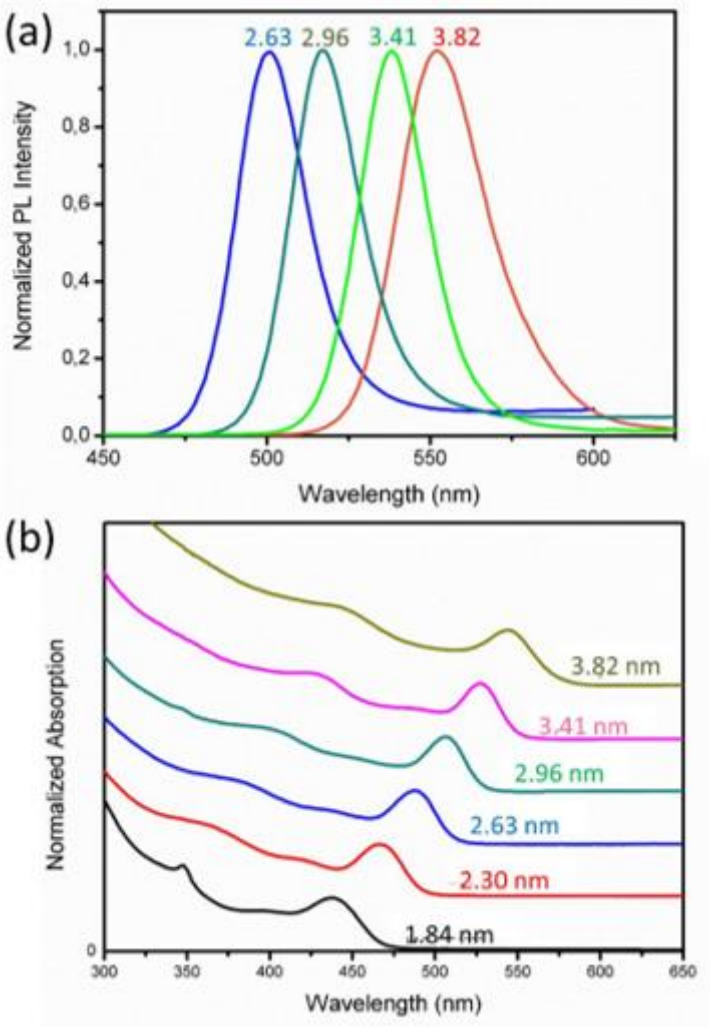

Figure 5.2 Emission (a) and absorption spectra of CdSe CQDs (b) synthesized at Demir Group laboratories, both showing size-dependent features [49]**.**

As observed in Figure 5.3, as a nanoparticle's size decreases, the energy difference between its valence band and conduction band increases, giving the color a deeper blue hue. The energy difference between the valence band and conduction band decreases for larger nanoparticles, shifting the glow toward red [96].

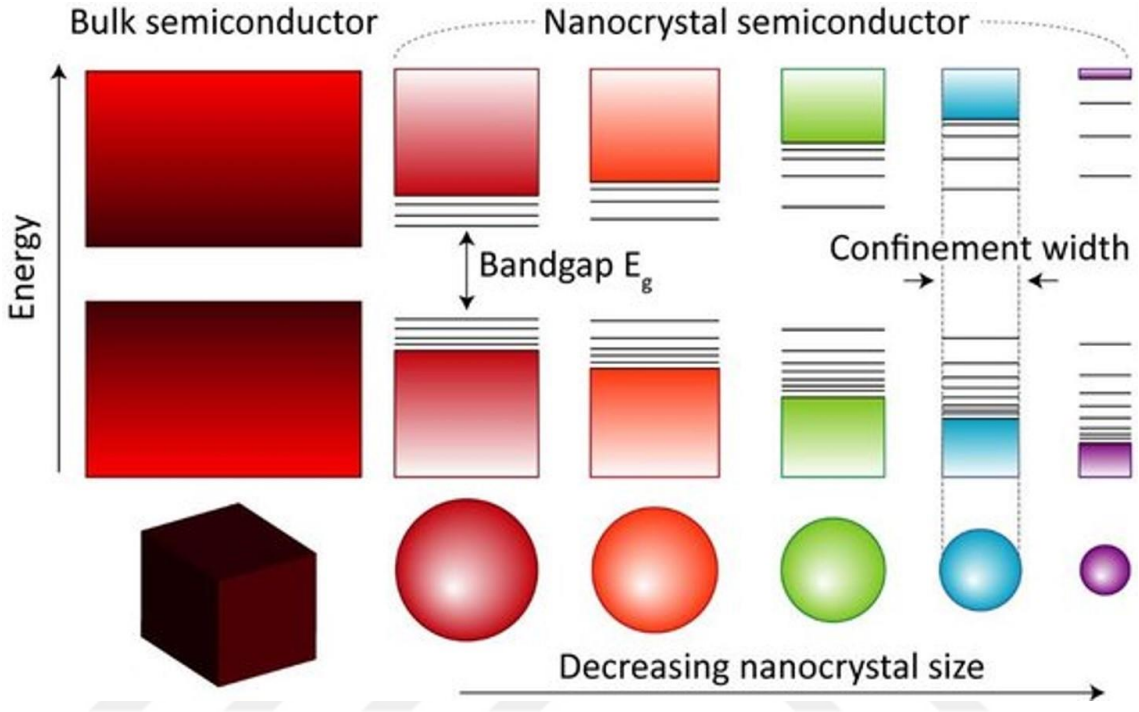

Figure 5.3 Schematic representation of quantum confinement effect. Comparison of bulk, and nanocrystals, indicating the size dependent bandgap of nanocrystals and the formation of discrete states near the band edge [95]**.**

The size of the semiconductor can be modified to control and modify a particle so that it can absorb or emit specific colors of light. However, in addition to their size, a CQD's properties are determined by their shape, structure, and composition. For instance, the shape of a quantum dot, which can be spherical, cubic, solid, or hollow, affects its properties. Additionally, the composition of CQDs can affect how well they operate. For instance, different quantum dot types (such as CdSe, CdS, ZnSe, InAs, and PbS) emit light with distinct emission spectra (UV, visible, or NIR), and the spectra can be controlled by changing the size and shape of the quantum dots. Therefore, by varying the size of the CQDs, the broad spectral range from UV to NIR can be covered, as illustrated in Figure 5.4, and this offers many advantages while designing optoelectronic devices [90].

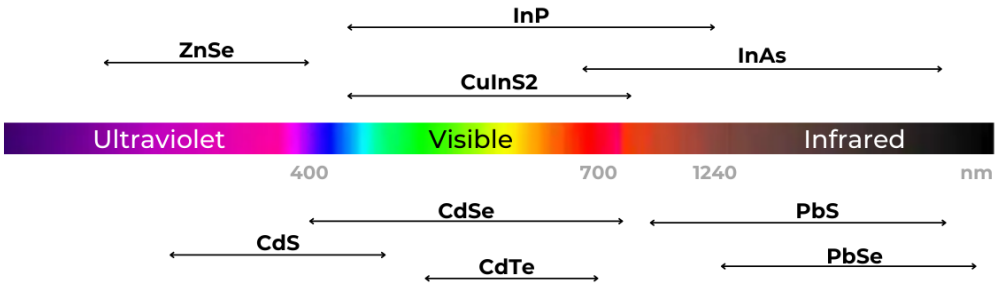

Figure 5.4 The spectral range of different types of QDs from UV to NIR.

Among these different types of colloidal quantum dots, CdSe- based core-shell heterostructures have been frequently used for luminesce in the visible range because of their narrow and symmetric emission reaching unity lineshape [100] and near-unity photoluminescence quantum yields (PLQY) [45],[101].

5.2 Synthesis techniques

To synthesize CQDs, a variety of techniques have been employed. Two synthesis approaches, the top-down approach and the bottom-up approach, stand out among these techniques. Reactive-ion etching, wet chemical etching, e-beam lithography, and X-ray lithography are examples of top-down processing methods. The major drawback of these methods that integration of impurities into the CQDs and structural imperfections by patterning [102],[103]. While the complexity and the need for expensive infrastructure are among the disadvantaged.

Many alternative self-assembly approaches have been utilized to synthesize CQDs using the bottom-up approach. These can be divided into two main categories: (i) wet chemical and (ii) vapor phase methods. There are several types of wet chemical techniques, including electrochemistry, hot-solution decomposition, competitive reaction chemistry, sol-gel, and microemulsion. These methods often follow standard precipitation procedures, where parameters are carefully controlled for a single solution or solution mixture. A number of vapor-phase techniques, including as molecular beam epitaxy (MBE), sputtering, and liquid metal ion sources, start with atom-by-atom layer growth. The CQDs subsequently self-assemble on a substrate without creating systems without creating any model [103]–[108]. In this thesis, we employed a one-pot reaction

to synthesize our red-emitting CQDs, and we followed the recipe that adapted from Altintas et al. [107].

5.2.1 Synthesis of CdSe/ZnS core/shell CQDs

Chemicals and Materials

Cadmium oxide (CdO, 99.99%), selenium (Se, 99.99% powder), sulfur (S, 99.998% trace metals basis), oleic acid (OA, 90% technical grade), 1-dodecanethiol (DDT, 98%), 1-octadecene (1-ODE, 90% technical grade), trioctylphosphine (TOP, 90% technical grade), methanol absolute (≥99.9%, Isolab), acetone (EMSURE, Merck), n-hexane (≥96%, Merck), and toluene (EMPLURA®). All chemicals and reagents were purchased from Sigma-Aldrich unless otherwise stated and used without further purification.

1 mmol CdO, 1.68 mmol $ZnAc{\cdot}2H_2O$ and 5 mL OA are added into a 50 mL round bottom flask and heated up to 130 °C under vacuum while stirring continuously. After 1 hour of degassing, the reaction is cooled down to 95 °C and 25 mL ODE is added to the flask. After completing an additional 30 min. of degassing at this temperature, the temperature is raised to 300 °C under nitrogen gas flow. 0.2 mL of 1 M TOP-Se hot injection solution, which is prepared in an argon-filled glovebox, is swiftly injected into the reaction flask. After 1.5 min., 300 μL DDT and 1 mL ODE are mixed in a vial and added to the reaction. At the end of 20 min., 1 mL of 2 M TOP-S solution, which is also prepared in the glovebox, is injected dropwise into the flask. The reaction ended after 10 minutes and cooled down to room temperature with air cooling. Synthesized QDs are purified by centrifugation at 5000 rpm for 10 min after adding acetone and methanol. The same cycle is repeated after redispersing in n-hexane. The final precipitate is redispersed in toluene and stored at 4 °C.

5.3 Optical properties of the CQDs

Also, absorbance and photoluminescence spectrum of synthesized red CdSe/ZnS core/shell CQDs provided in Figure 5.5. As it can be clearly seen from the Figure 5.5, the intrinsic PL of the synthesized CQDs overlaps with the absorption spectrum. While the resulting PL peak wavelength of the synthesized CQDs was at 619 nm, the quantum efficiency was measured as 55.7 %. Additionally, we report that the photoluminescence FWHM was determined as 28 nm.

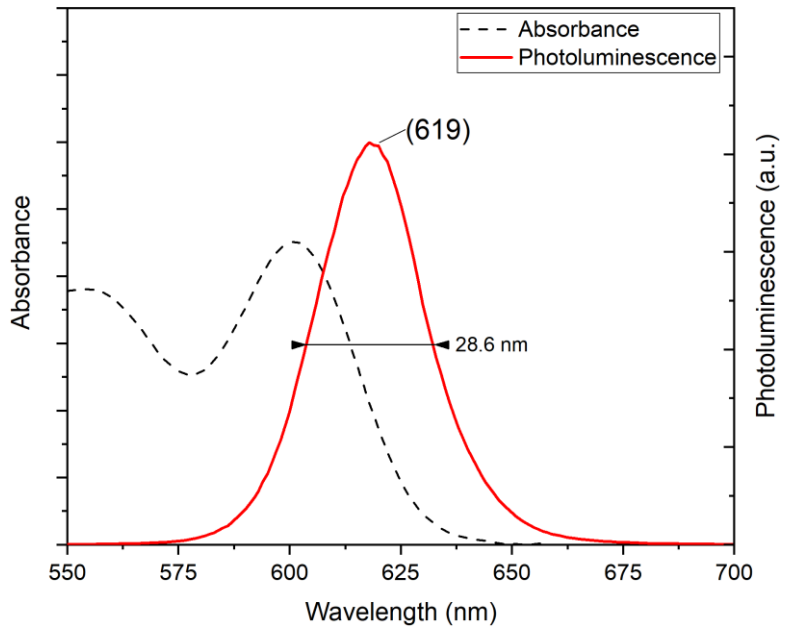

Figure 5.5 The absorbance and photoluminescence spectrum of synthesized red CdSe/ZnS core/shell CQDs.

Chapter 6

Fabrication of solution processed CQD photodetectors

With an emphasis on developing sustainable methods for fabricating optoelectronic devices, here we report a simple methodology to realize solution-processed colloidal quantum dot photodetectors (CQD PDs) operating in visible regime.

6.1 Sample fabrication

The fabrication of the photodetectors starts with cleaning 2.5x2.5 cm^2 glass substrates. They were first sonicated in 2-propanol for 7 min and then treated in a Harrick Plasma Expanded Plasma Cleaner System for another 7 min.

Subsequently, Ag NW (2 mg mL^{-1} in ethanol) were spin-coated onto the cleaned glass substrate at 2000 rpm for 60 s. The deposition procedure was repeated 10 times to obtain a transparent and conductive film as described in Chapter 3. The substrate was then annealed at 150 °C for 15 min. The fabrication process continued with spin-coating of ZnO NPs (5 mg mL^{-1} in ethanol) at 1000 rpm for 30 s. Next, the substrate was annealed at 150 °C for 20 min. In an effort to deposit CdSe/ZnS CQDs between the Ag NW electrodes, a gap of width ~30 μm was opened by mechanically scratching the Ag NW-ZnO film using a surgical blade that had been heated using the tip of a soldering iron prior to scratching.

Finally, the semiconducting CdSe/ZnS CQDs (20 mg mL^{-1} in toluene) were drop-casted onto this gap and annealed at 60 °C for 15 min. The whole fabrication that illustrated in Figure 6.1 was carried out under ambient air conditions. Also, Figure 6.2 shows that the photo of final device structure.

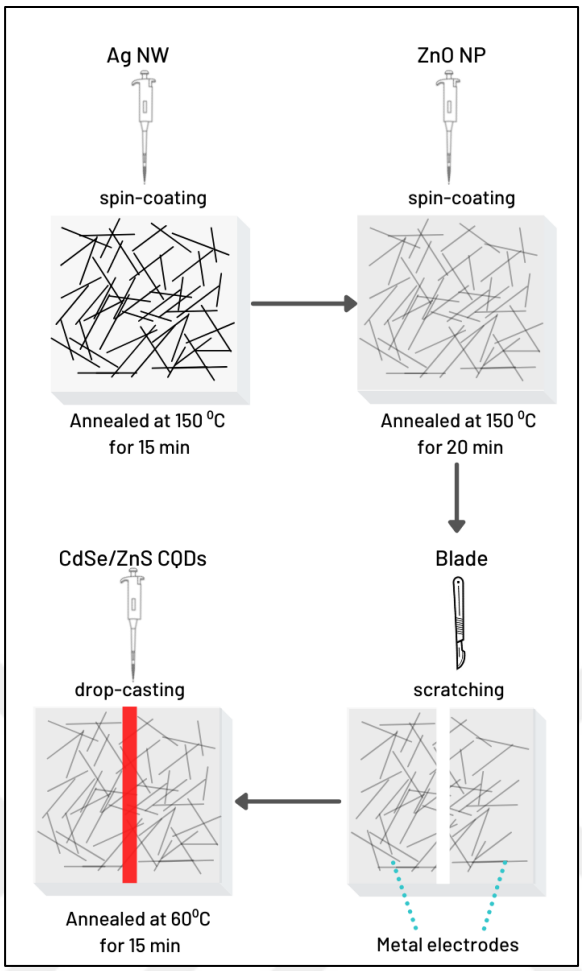

Figure 6.1 The illustration of the proposed fabrication procedure to obtain metal-semiconductor-metal quantum dot photodetectors.

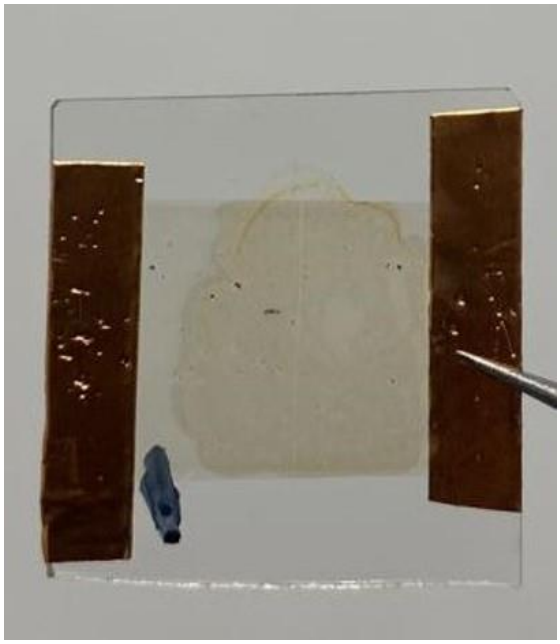

Figure 6.2 The photo of the proposed fabrication procedure to obtain metal-semiconductor-metal quantum dot photodetectors.

Upon preparing the conductive parts of the metal-semiconductor-metal photodetector, the semiconductor portion of the device was obtained using red-emitting colloidal quantum dots that are synthesized as described in the Chapter 5. Before placing these quantum dots, a gap between the conductive parts is necessary. Conventional methods involve the use of lithography that requires costly infrastructure and consumes a significant amount of energy. In this thesis, as an alternative to lithography, we opened the gap by scratching the conductive films using a simple blade. For this purpose, several blade types including razor blade knives and several sizes of syringe tips were tried. Following the gap formation, we drop-casted the CQDs on the gap and measured the photocurrent. We observed that among various types of blades we employed only the surgical blade of # 11 (or No.11) allowed the detection of the photocurrent. Moreover, when we scratch the Ag NW films by using the blade, we realized that Ag NW residues may remain in the gap. Heating the surgical blade at 150 ºC for 5 min before scratching the film enabled a reliable and higher photocurrent reading (Figure 6.3 (b)). We observed that scratching the Ag NW-ZnO NP film via a surgical blade opened a gap of ~30 μm (Figure 6.3 (d)).

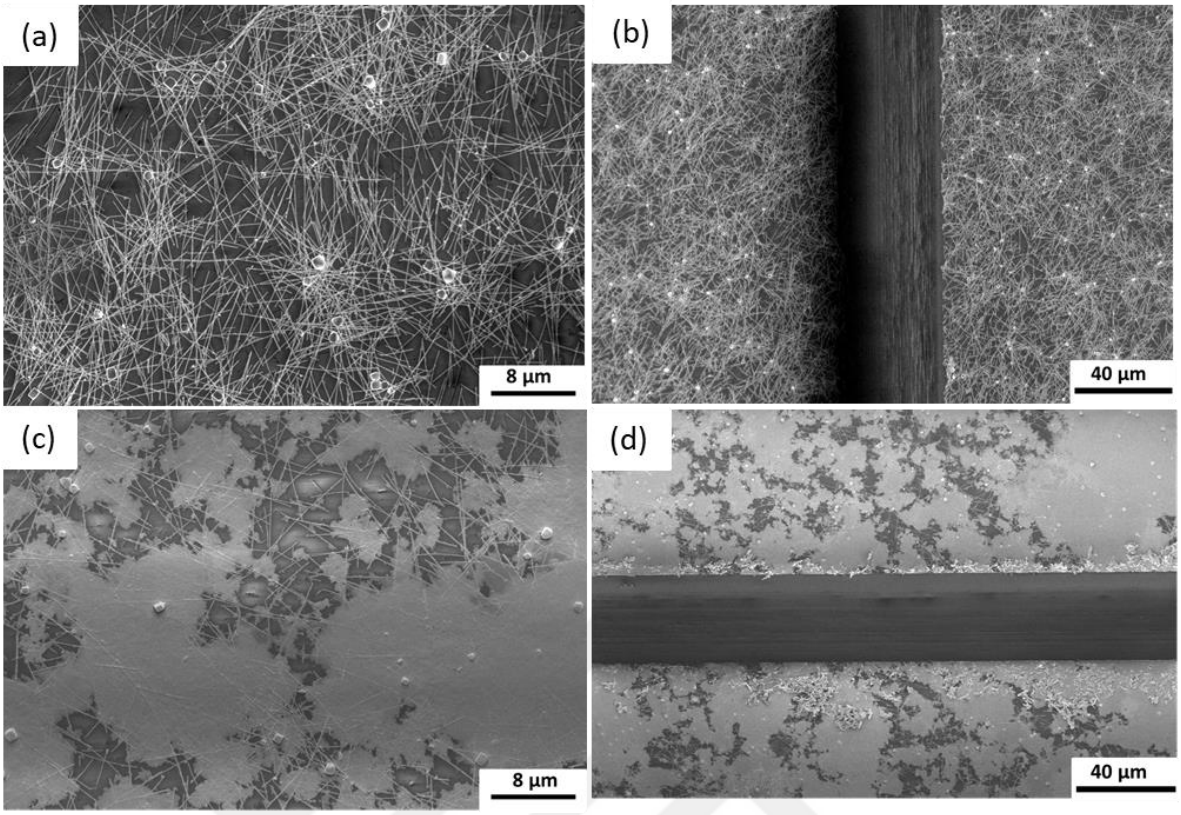

Figure 6.3 SEM images of Ag NW-ZnO electrodes. (a) Structure of Ag NW films without scratching. (b) Structure of Ag NW films after scratching with some residuals. (c) Structure of Ag NW-ZnO films without scratching. (d) Structure of Ag NW-ZnO films after scratching with almost no residuals of Ag NW.

6.2 Characterization

Transmittance measurements were taken by using a Thermo 10S UV-vis spectrometer. Sheet resistance was measured by using a homemade four-point probe. Five different points were measured for each sample and the average value was reported. The surface of the films was imaged by using a Zeiss Gemini scanning electron microscope (SEM). Current-voltage and responsivity measurements were taken using a Keithley 2400 source meter illuminated by a monochromator-equipped broadband light source as illustrated in Figure 6.4.

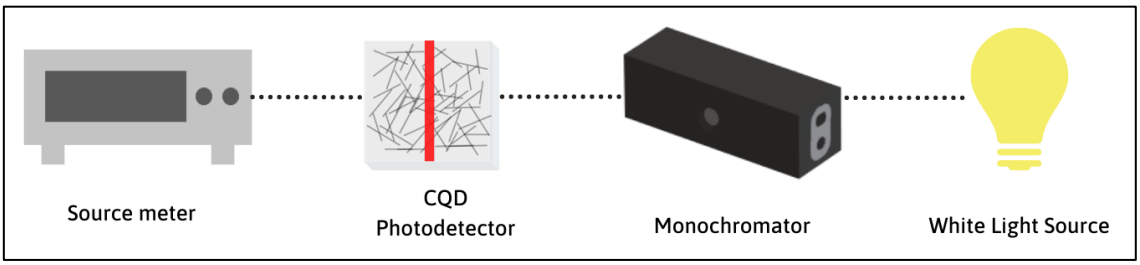

Figure 6.4 Schematics of the responsivity measurement setup. Voltage is applied to the photodetector while measuring the photocurrent under illumination at different wavelengths between 400 and 650 nm that are generated with the help of a white light source and a monochromator.

6.3 Results and Discussion

As the active layer of the photodetector, we drop-casted red-emitting CdSe/ZnS core/shell CQDs (20 mg mL^{-1} in toluene) onto this gap to form a metal-semiconductor-metal photodetector and the thickness of this CQD film was several tens of micrometers. Next, we measured the photocurrent by exciting the CQDs at various wavelengths under different bias voltages. To quantitatively evaluate the performance of the device, both responsivity (R) and detectivity (D*) of the photodetector were calculated.

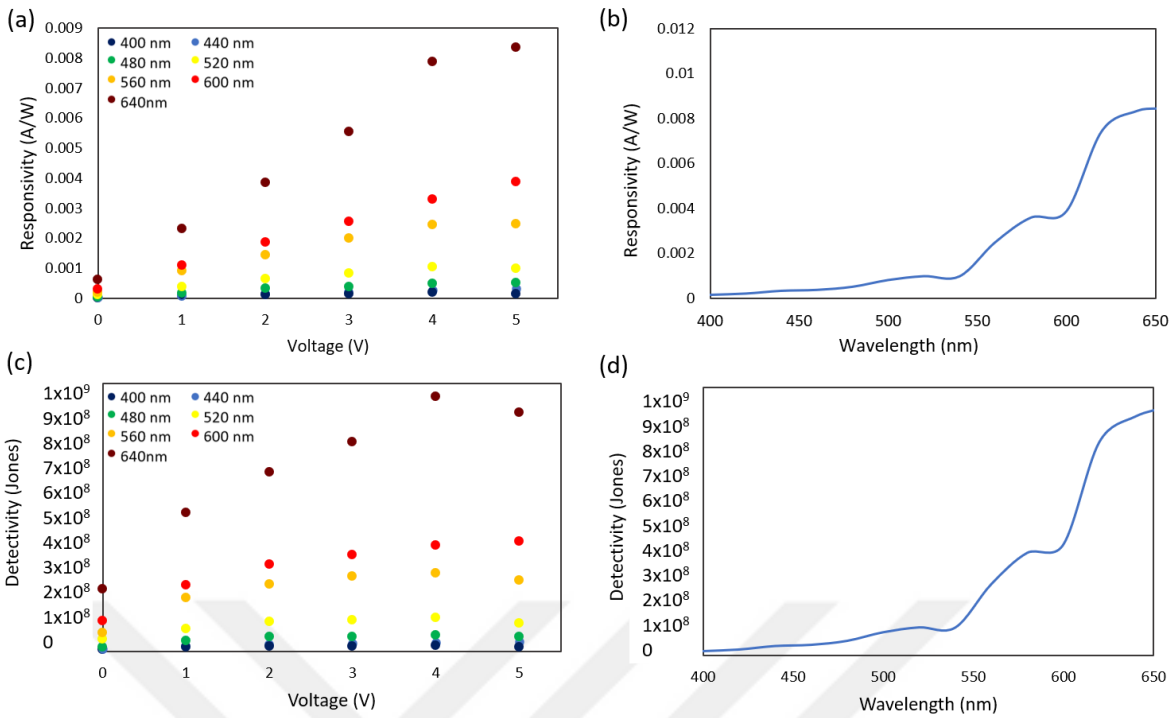

Figure 6.5 (a) The responsivity of the photodetectors at different bias voltages in the range of 400-640 nm. (b) The responsivity spectrum of photodetectors at a bias voltage of 5 V as a function of wavelength. (c) The detectivity of the photodetectors at different bias voltages in the range of 400-640 nm. (d) The detectivity spectrum of photodetectors at a bias voltage of 5 V as a function of wavelength.

As it can be seen in Figure 6.5 (a), the responsivity of the photodetectors strongly depends on the applied bias and the wavelength. The maximum responsivity and detectivity of the devices were recorded at a bias of 5 V as ~8.5 mA/W and ~0.95×10^9 Jones, respectively. With increasing voltage, the strengthened electric field between the electrodes makes it easier to collect charges leading to increased photocurrent and responsivity. As shown in Figure 6.5 (b), the responsivity of the PD is also a strong function of the wavelength. When we compare this dependence with the absorbance of the CQDs, we realize that the responsivity drops at shorter wavelengths as opposed to the absorbance of the CQDs that increases with shortening wavelengths. This shows us that the generated electron-hole pairs at shorter wavelength exposures cannot be collected by the contacts as efficiently as in the case of longer wavelengths. We attribute this difference to the large thickness of the CQD layer occurring due to the drop-casting method. Since the light at shorter wavelengths will be absorbed more strongly by the CQDs, the penetration depth of the short-wavelength-light is much smaller compared to the light at longer wavelengths. Also, the highly energetic photons

are absorbed just at the first few microns of the top part of the device and cannot reach to the active region to be harvested. As a result, the excitons generated by the light at shorter wavelengths will remain away from the Ag NW contacts making it difficult to collect the carriers, which consequently decreases the responsivity of the PD. In Figure 6.5 (a), and 6.5 (c), we see that the responsivity and the detectivity of the photodiode has an almost linear dependence on the applied bias. This shows that the collected photocurrent mainly relies on the photoresistive effect. When the photodetector is illuminated with light, the increased number of charge carriers decreases the resistance of the CQD layer. The fact that the photocurrent or resistivity vs. applied bias relation is linear indicates that the total number of charge carriers is controlled by the light rather than the applied bias within the voltage range of interest (0-5 V). Our devices are fabricated for applications that do not require very high responsivities and detectivities. When we compare our devices with the other photodetectors that are fabricated using environmentally hazardous, costly and energy-consuming methods, we can see that their detectivity values reaching $>10^{14}$ Jones [110]–[113] and responsivities up to $>10^{3}$ A/W [114]–[117] in the visible region. Those devices can be used for applications that require high responsivities and detectivities.

Chapter 7

Conclusions and Future Prospects

7.1 Conclusions

In this work, we successfully fabricated solution-processed quantum dot photodetectors with a metal-semiconductor-metal structure which has the simplest architecture as they involve only a semiconductor material sandwiched between two electrodes. To eliminate the need for metal evaporation or sputtering and photolithography during the electrode fabrication, we opened the gap between electrodes using a simple surgical blade. We started the fabrication by spin-coating Ag NW onto glass substrates with a sheet resistance of 180 Ω/□. In order to improve the Ag NW adhesion on substrate and conductivity, we spin-coated zinc oxide nanoparticles (ZnO NP) on Ag NW network. These conductive films exhibited a low sheet resistance (95 Ω/□) in addition to high optical transparencies (greater than 70%). To fabricate highly conductive films with high transparency, we investigated the effect of annealing temperature on the conductivity of the films and we fixed the annealing temperature at 150 ºC since the results indicate that annealing the films at 150 ºC yields the lowest sheet resistance. After preparing the conductive parts of the metal-semiconductor-metal photodetector, we opened a gap between the conductive parts using a simple blade instead of conventional methods that require the use of lithography which is a costly infrastructure in addition to the wastes generated. SEM images indicated that scratching the Ag NW-ZnO NP film via a surgical blade opened a gap of ~30 μm. After their synthesis, these colloidal quantum dots were simply drop-casted onto the gap opened on the conductive film, finishing the metal-semiconductor-metal photodetector architecture. These visible CQD-based photodetectors exhibited responsivities and detectivities up to 8.5 mA/W and 0.95×10^9 Jones, respectively, at a bias voltage of 5 V and wavelength of 650 nm. These proof-of-concept photodetectors show that light-harvesting devices can be obtained using the environmentally friendly, low-cost, and

energy-saving technique presented here rather than the conventional energy-hungry and costly methods.

7.2 Societal Impact and Contribution to Global Sustainability

Photodetectors (PDs) are among the most widely used optoelectronic devices that find various applications in a variety of fields including commercial electronics, imaging, communications, and military equipment [50]. Such diverse applications bring together the need for certain specifications depending on the purpose of use. Such differences in the application requirements triggered the use of various active region materials [116] as well as device architectures [10].

Fabrication of these photodetectors relies on conventional tools such as chemical vapor deposition, lithography, and metal evaporation [117]–[119]. These tools and techniques are expensive, energy-consuming and employ toxic chemicals [120]. Furthermore, the thin films in these devices are usually deposited at elevated temperatures and under high vacuum which impose further restrictions on the device fabrication. Along with their increased energy consumption, the fabrication process of the photodetectors, like most the other electronic and optoelectronic devices, has benign effects on the environment. Developing an alternative technology would contribute to the efforts on achieving a sustainable optoelectronics technology.

With an emphasis on developing sustainable methods for fabricating optoelectronic devices, in this thesis we reported a simple methodology to realize solution-processed colloidal quantum dot photodetectors (CQD PDs) operating in visible regime. As long as the application requirements allow for it, simplifying the device fabrication would contribute to realizing a more sustainable optoelectronics technology.

Among various photodetector types, metal-semiconductor-metal photodetectors have the simplest architecture as they involve only a semiconductor material sandwiched between two electrodes. Nevertheless, these electrodes are often obtained using photolithography and metal evaporation or sputtering which are costly and energy-consuming. Instead of using these techniques, we employed silver nanowires (Ag NW) as the transparent electrodes replacing the indium-tin-oxide (ITO) commonly

used in optoelectronic devices to fabricate these fully solution-processed and transparent metal-semiconductor-metal photodetectors.

The attempts to decrease the environmental footprint of the optoelectronic device fabrication should involve the materials within the active region and the electrodes. Silicon and germanium step forward as the most widely used semiconductors used in the active region of the photodetectors [121]. However, their growth process is far from being environmentally friendly [122]. An alternative to them, we employed colloidal quantum dots (CQDs) which are solution-processed materials that most of the time simply require a spin-coating process.

These proof-of-concept photodetectors showed that the environmentally friendly, low-cost, and energy-saving technique presented here can be an alternative to conventional, high-cost, and energy-hungry techniques while fabricating light-harvesting devices.

7.3 Future Prospects

As it was mentioned in previous, photodetectors are most widely used optoelectronic devices in many areas. Fabrication of commercial photodetectors are generally required expensive and energy-consuming tools. With this environmentally friendly, and low-cost fabrication method that we utilized to fabricated our photodetectors, biofriendly detectors can be manufactured. Also, one can fabricate commercial cameras through using these photodetectors since they are operated in visible regime.

BIBLIOGRAPHY

[1] M. Savas, A. F. Yazici, A. Arslan, E. Mutlugün, and T. Erdem, "Simple, sustainable fabrication of fully solution-processed, transparent, metal-semiconductor-metal photodetectors using a surgical blade as an alternative to conventional tools," *https://doi.org/10.1117/12.2621385*, vol. 12131, pp. 181–193, May 2022, doi: 10.1117/12.2621385.

[2] P. C. Y. Chow, T. Someya, P. C. Y. Chow, and T. Someya, "Organic Photodetectors for Next-Generation Wearable Electronics," *Advanced Materials*, vol. 32, no. 15, p. 1902045, Apr. 2020, doi: 10.1002/ADMA.201902045.

[3] M. bin Lien *et al.*, "Ranging and light field imaging with transparent photodetectors," *Nature Photonics 2020 14:3*, vol. 14, no. 3, pp. 143–148, Jan. 2020, doi: 10.1038/s41566-019-0567-3.

[4] Z. Zhao, J. Liu, Y. Liu, and N. Zhu, "High-speed photodetectors in optical communication system *," *Journal of Semiconductors*, vol. 38, no. 12, p. 121001, Dec. 2017, doi: 10.1088/1674-4926/38/12/121001.

[5] M. Kataria *et al.*, "Highly Sensitive, Visible Blind, Wearable, and Omnidirectional Near-Infrared Photodetectors," *ACS Nano*, vol. 12, no. 9, pp. 9596–9607, Sep. 2018, doi: 10.1021/ACSNANO.8B05582/SUPPL_FILE/NN8B05582_SI_001.PDF.

[6] M. M. Ackerman, X. Tang, and P. Guyot-Sionnest, "Fast and Sensitive Colloidal Quantum Dot Mid-Wave Infrared Photodetectors," *ACS Nano*, vol. 12, no. 7, pp. 7264–7271, Jul. 2018, doi: 10.1021/ACSNANO.8B03425/SUPPL_FILE/NN8B03425_SI_001.PDF.

[7] G. Konstantatos, J. Clifford, L. Levina, and E. H. Sargent, "Sensitive solution-processed visible-wavelength photodetectors," *Nature Photonics 2007 1:9*, vol. 1, no. 9, pp. 531–534, Sep. 2007, doi: 10.1038/nphoton.2007.147.

[8] P. Ma *et al.*, "Fast MoTe2 Waveguide Photodetector with High Sensitivity at Telecommunication Wavelengths," *ACS Photonics*, vol. 5, no. 5, pp. 1846–1852, May 2018, doi: 10.1021/ACSPHOTONICS.8B00068/SUPPL_FILE/PH8B00068_SI_001.PDF.

[9] K. Xu, W. Zhou, Z. Ning, K. Xu, W. Zhou, and Z. Ning, "Integrated Structure and Device Engineering for High Performance and Scalable Quantum Dot Infrared Photodetectors," *Small*, vol. 16, no. 47, p. 2003397, Nov. 2020, doi: 10.1002/SMLL.202003397.

[10] S. O. Kasap, "Optoelectronics and Photonics: Principles and Practices," *Prentice Hall, 1st edition*, p. 340, 2001, Accessed: Dec. 14, 2021. [Online]. Available: https://books.google.com/books?id=7MMVPwAACAAJ&pgis=1

[11] J. P. Clifford, G. Konstantatos, K. W. Johnston, S. Hoogland, L. Levina, and E. H. Sargent, "Fast, sensitive and spectrally tuneable colloidal-quantum-dot photodetectors," *Nature Nanotechnology 2009 4:1*, vol. 4, no. 1, pp. 40–44, Nov. 2008, doi: 10.1038/nnano.2008.313.

[12] E. J. D. Klem, C. W. Gregory, G. B. Cunningham, S. Hall, D. S. Temple, and J. S. Lewis, "Planar PbS quantum dot/C60 heterojunction photovoltaic devices with 5.2% power conversion efficiency," *Applied Physics Letters*, vol. 100, no. 17, p. 173109, Apr. 2012, doi: 10.1063/1.4707377.

[13] J. W. Lee, D. Y. Kim, and F. So, "Unraveling the Gain Mechanism in High Performance Solution-Processed PbS Infrared PIN Photodiodes," *Advanced*

Functional Materials, vol. 25, no. 8, pp. 1233–1238, Feb. 2015, doi: 10.1002/ADFM.201403673.

[14] C. Xue *et al.*, "Fabrication of large-area high-aspect-ratio periodic nanostructures on various substrates by soft X-ray interference lithography," *Applied Surface Science*, vol. 425, pp. 553–557, Dec. 2017, doi: 10.1016/J.APSUSC.2017.07.010.

[15] W. Tian *et al.*, "Low-dimensional nanomaterial/Si heterostructure-based photodetectors," *InfoMat*, vol. 1, no. 2, pp. 140–163, Jun. 2019, doi: 10.1002/INF2.12014.

[16] J. Michel, J. Liu, and L. C. Kimerling, "High-performance Ge-on-Si photodetectors," *Nature Photonics 2010 4:8*, vol. 4, no. 8, pp. 527–534, Jul. 2010, doi: 10.1038/nphoton.2010.157.

[17] R. Dong *et al.*, "High-Gain and Low-Driving-Voltage Photodetectors Based on Organolead Triiodide Perovskites," *Advanced Materials*, vol. 27, no. 11, pp. 1912–1918, Mar. 2015, doi: 10.1002/ADMA.201405116.

[18] C. Livache *et al.*, "A colloidal quantum dot infrared photodetector and its use for intraband detection," *Nature Communications 2019 10:1*, vol. 10, no. 1, pp. 1–10, May 2019, doi: 10.1038/s41467-019-10170-8.

[19] P. Sen *et al.*, "Panchromatic All-Polymer Photodetector with Tunable Polarization Sensitivity," *Advanced Optical Materials*, vol. 7, no. 4, p. 1801346, Feb. 2019, doi: 10.1002/ADOM.201801346.

[20] Y. Xu and Q. Lin, "Photodetectors based on solution-processable semiconductors: Recent advances and perspectives," *Applied Physics Reviews*, vol. 7, no. 1, p. 011315, Mar. 2020, doi: 10.1063/1.5144840.

[21] J. Kim *et al.*, "A skin-like two-dimensionally pixelized full-color quantum dot photodetector," *Science Advances*, vol. 5, no. 11, Nov. 2019, doi: 10.1126/SCIADV.AAX8801/SUPPL_FILE/AAX8801_SM.PDF.

[22] G. Konstantatos and E. H. Sargent, "Solution-Processed Quantum Dot Photodetectors Perovskties for light emission View project Halide perovskites photovoltaics View project Solution-Processed Quantum Dot Photodetectors Flexible thin-film photodetectors for imaging systems, including those suitable for video applications, can handle visible light and also enter the infrared spectral region," 2009, doi: 10.1109/JPROC.2009.2025612.

[23] L. Pan, S. Shrestha, N. Taylor, W. Nie, and L. R. Cao, "Determination of X-ray detection limit and applications in perovskite X-ray detectors", doi: 10.1038/s41467-021-25648-7.

[24] N. Li, P. Mahalingavelar, J. H. Vella, D. S. Leem, J. D. Azoulay, and T. N. Ng, "Solution-processable infrared photodetectors: Materials, device physics, and applications," *Materials Science and Engineering R: Reports*, vol. 146, Oct. 2021, doi: 10.1016/J.MSER.2021.100643.

[25] G. Konstantatos, J. Clifford, L. Levina, and E. H. Sargent, "Sensitive solution-processed visible-wavelength photodetectors," 2007, doi: 10.1038/nphoton.2007.147.

[26] J. Wang and S. Lee, "Ge-Photodetectors for Si-Based Optoelectronic Integration," *Sensors*, vol. 11, pp. 696–718, 2011, doi: 10.3390/s110100696.

[27] W.-Y. Kong *et al.*, "Graphene-β-Ga2O3 Heterojunction for Highly Sensitive Deep UV Photodetector Application," *Advanced Materials*, vol. 28, no. 48, pp. 10725–10731, Dec. 2016, doi: 10.1002/ADMA.201604049.

[28] "Photodetectors, explained by RP Photonics Encyclopedia; photodiodes, phototransistors, pyroelectric photodetectors, array, power meter, noise." https://www.rp-photonics.com/photodetectors.html (accessed Jul. 04, 2022).

[29] “Photodiode - Symbol, Working and Types - Diode.” https://www.physics-and-radio-electronics.com/electronic-devices-and-circuits/semiconductor-diodes/photodiodesymboltypes.html (accessed Jun. 23, 2022).
[30] V. I. Blynskii, Y. G. Vasileuskii, S. A. Malyshev, and A. L. Chizh, “Silicon photodiode with a grid p-n junction,” *Semiconductors 2007 41:2*, vol. 41, no. 2, pp. 223–226, Feb. 2007, doi: 10.1134/S1063782607020200.
[31] “PHOTODIODE BASICS – Wavelength Electronics.” https://www.teamwavelength.com/photodiode-basics/ (accessed Jun. 23, 2022).
[32] A. H. Wilson, “The internal photoelectric effect in crystals,” *Nature*, vol. 130, no. 3294, pp. 913–915, 1932, doi: 10.1038/130913A0.
[33] “Photodiode - Wikipedia.” https://en.wikipedia.org/wiki/Photodiode (accessed Jun. 23, 2022).
[34] J. Taylor *et al.*, “Characterization of Power-to-Phase Conversion in High-Speed P-I-N”.
[35] I. Kimukin, N. Biyikli, O. Aytur, S. M. Ünlü, and E. Ozbay, “InGaAs-Based High-Performance p-i-n Photodiodes,” *IEEE PHOTONICS TECHNOLOGY LETTERS*, vol. 14, no. 3, 2002, Accessed: Jul. 04, 2022. [Online]. Available: http://www.newport.com
[36] “PIN diode - Wikipedia.” https://en.wikipedia.org/wiki/PIN_diode#Applications (accessed Jun. 26, 2022).
[37] “PN Photodiode & PIN Photo Diode » Electronics Notes.” https://www.electronics-notes.com/articles/electronic_components/diode/photodiode-detector-pn-pin.php (accessed Jun. 26, 2022).
[38] “What is PIN Photodiode ? | It’s 5+ Important use and characteristics.” https://lambdageeks.com/pin-photodiode/ (accessed Jun. 26, 2022).
[39] “Avalanche Photodiode : Construction, Working & Its Applications.” https://www.elprocus.com/avalanche-photodiode/ (accessed Jun. 27, 2022).
[40] “Avalanche Photodiode | Its 5+ Important uses and characteristics.” https://lambdageeks.com/avalanche-photodiodes/ (accessed Jun. 27, 2022).
[41] J. C. Campbell *et al.*, “Recent Advances in Avalanche Photodiodes,” *IEEE JOURNAL OF SELECTED TOPICS IN QUANTUM ELECTRONICS*, vol. 10, no. 4, p. 777, 2004, doi: 10.1109/JSTQE.2004.833971.
[42] “Avalanche photodiode: function, behavior, industries.” https://www.first-sensor.com/en/products/optical-sensors/detectors/avalanche-photodiodes-apd/ (accessed Jun. 27, 2022).
[43] R. S. Quimby, “Photonics and Lasers: An Introduction,” *Photonics and Lasers: An Introduction*, pp. 1–519, May 2006, doi: 10.1002/0471791598.
[44] “Schottky Photodiode: Schottky Photo Detector » Electronics Notes.” https://www.electronics-notes.com/articles/electronic_components/diode/photodiode-detector-schottky.php (accessed Jul. 04, 2022).
[45] M. Liu, N. Yazdani, M. Yarema, M. Jansen, V. Wood, and E. H. Sargent, “Colloidal quantum dot electronics,” *Nature Electronics*, 1928, doi: 10.1038/s41928-021-00632-7.
[46] C. Li, Y. Ma, Y. Xiao, L. Shen, and L. Ding, “Advances in perovskite photodetectors,” 2020, doi: 10.1002/inf2.12141.
[47] S. Miao and Y. Cho, “Toward Green Optoelectronics: Environmental-Friendly Colloidal Quantum Dots Photodetectors,” 2019, doi: 10.3389/fenrg.2021.666534.

[48] P. Reiss, M. Protière, and L. Li, "Core/Shell semiconductor nanocrystals," *Small*, vol. 5, no. 2, pp. 154–168, Jan. 2009, doi: 10.1002/SMLL.200800841.
[49] T. Erdem and H. V. Demir, "Color science of nanocrystal quantum dots for lighting and displays," *Nanophotonics*, vol. 2, no. 1, pp. 57–81, Feb. 2013, doi: 10.1515/NANOPH-2012-0031/ASSET/GRAPHIC/NANOPH-2012-0031_FIG27.JPG.
[50] E. H. Sargent and G. Konstantatos, "Solution-Processed Quantum Dot Photodetectors Solution-Processed Quantum Dot Photodetectors Flexible thin-film photodetectors for imaging systems, including those suitable for video applications, can handle visible light and also enter the infrared spectral region," 2009, doi: 10.1109/JPROC.2009.2025612.
[51] Q. Xu, L. Meng, K. Sinha, F. I. Chowdhury, J. Hu, and X. Wang, "Ultrafast Colloidal Quantum Dot Infrared Photodiode," vol. 12, p. 38, 2022, doi: 10.1021/acsphotonics.0c00363.
[52] Y. Tang *et al.*, "A Colloidal-Quantum-Dot Infrared Photodiode with High Photoconductive Gain," *Small*, vol. 14, no. 48, p. 1803158, Nov. 2018, doi: 10.1002/SMLL.201803158.
[53] S. Kim, E. Kim, J. Hwang, S.-E. Park, and D.-Y. Lee, "Fabrication of Silver Nanowire Transparent Electrodes using Electrohydrodynamic Spray Deposition for Flexible Organic Solar Cells Fabrication of silver nanowire transparent electrodes using electrohydrodynamic spray deposition for flexible organic solar cells †," *Article in Journal of Materials Chemistry*, 2013, doi: 10.1039/C3TA13204H.
[54] X. Huang *et al.*, "Super-Stretchable and Self-Healing hydrogel with a Three-Dimensional silver nanowires network structure for wearable sensor and electromagnetic interference shielding," *Chemical Engineering Journal*, vol. 446, p. 137136, Oct. 2022, doi: 10.1016/J.CEJ.2022.137136.
[55] T. Tokuno *et al.*, "Fabrication of Silver Nanowire Transparent Electrodes at Room Temperature," *Nano Res*, vol. 4, no. 12, pp. 1215–1222, 2011, doi: 10.1007/s12274-011-0172-3.
[56] B. J. Murray, Q. Li, J. T. Newberg, J. C. Hemminger, and R. M. Penner, "Silver oxide microwires: Electrodeposition and observation of reversible resistance modulation upon exposure to ammonia vapor," *Chemistry of Materials*, vol. 17, no. 26, pp. 6611–6618, Dec. 2005, doi: 10.1021/CM051647R/ASSET/IMAGES/LARGE/CM051647RF00006.JPEG.
[57] P. Zhang *et al.*, "Silver nanowires: Synthesis technologies, growth mechanism and multifunctional applications," *Materials Science and Engineering B: Solid-State Materials for Advanced Technology*, vol. 223, pp. 1–23, Sep. 2017, doi: 10.1016/J.MSEB.2017.05.002.
[58] D. S. Hecht, L. Hu, and G. Irvin, "Emerging Transparent Electrodes Based on Thin Films of Carbon Nanotubes, Graphene, and Metallic Nanostructures," *Advanced Materials*, vol. 23, no. 13, pp. 1482–1513, Apr. 2011, doi: 10.1002/ADMA.201003188.
[59] B. Li, S. Ye, I. E. Stewart, S. Alvarez, and B. J. Wiley, "Synthesis and Purification of Silver Nanowires to Make Conducting Films with a Transmittance of 99%," *Nano Letters*, vol. 15, no. 10, pp. 6722–6726, Oct. 2015, doi: 10.1021/ACS.NANOLETT.5B02582/ASSET/IMAGES/LARGE/NL-2015-02582X_0002.JPEG.

[60] S. Hou, J. Liu, F. Shi, G.-X. Zhao, J.-W. Tan, and G. Wang, “Recent Advances in Silver Nanowires Electrodes for Flexible Organic/ Perovskite Light-Emitting Diodes”, doi: 10.3389/fchem.2022.864186.

[61] D. Tan, C. Jiang, Q. Li, S. Bi, and J. Song, “Silver nanowire networks with preparations and applications: a review,” *Journal of Materials Science: Materials in Electronics*, vol. 31, no. 18, pp. 15669–15696, Sep. 2020, doi: 10.1007/S10854-020-04131-X/FIGURES/25.

[62] M. Mazur, “Electrochemically prepared silver nanoflakes and nanowires,” *Electrochemistry Communications*, vol. 4, no. 6, pp. 400–403, Apr. 2004, doi: 10.1016/J.ELECOM.2004.02.011.

[63] T. D. Lazzara, G. R. Bourret, R. B. Lennox, and T. G. M. van de Ven, “Polymer templated synthesis of AgCN and Ag nanowires,” *Chemistry of Materials*, vol. 21, no. 10, pp. 2020–2026, May 2009, doi: 10.1021/CM802481V/SUPPL_FILE/CM802481V_SI_001.PDF.

[64] D. Zhang, L. Qi, J. Ma, and H. Cheng, “Formation of silver nanowires in aqueous solutions of a double-hydrophilic block copolymer,” *Chemistry of Materials*, vol. 13, no. 9, pp. 2753–2755, 2001, doi: 10.1021/CM0105007/ASSET/IMAGES/LARGE/CM0105007F00003.JPEG.

[65] Y. Sun, B. Gates, B. Mayers, and Y. Xia, “Crystalline Silver Nanowires by Soft Solution Processing,” *Nano Letters*, vol. 2, no. 2, pp. 165–168, Feb. 2002, doi: 10.1021/NL010093Y/ASSET/IMAGES/LARGE/NL010093YF00004.JPEG.

[66] T. Kim, A. Canlier, G. H. Kim, J. Choi, M. Park, and S. M. Han, “Electrostatic Spray Deposition of Highly Transparent Silver Nanowire Electrode on Flexible Substrate,” *ACS Applied Materials and Interfaces*, vol. 5, no. 3, pp. 788–794, Feb. 2013, doi: 10.1021/AM3023543.

[67] M. M. Ghorbani and R. Taherian, “Methods of measuring electrical properties of material,” *Electrical Conductivity in Polymer-Based Composites: Experiments, Modelling, and Applications*, pp. 365–394, Jan. 2018, doi: 10.1016/B978-0-12-812541-0.00012-4.

[68] H. Kim *et al.*, “Electrical, optical, and structural properties of indium–tin–oxide thin films for organic light-emitting devices,” *Journal of Applied Physics*, vol. 86, no. 11, p. 6451, Nov. 1999, doi: 10.1063/1.371708.

[69] G. R. S. Andrade, C. C. Nascimento, Z. M. Lima, E. Teixeira-Neto, L. P. Costa, and I. F. Gimenez, “Star-shaped ZnO/Ag hybrid nanostructures for enhanced photocatalysis and antibacterial activity,” *Applied Surface Science*, vol. 399, pp. 573–582, Mar. 2017, doi: 10.1016/J.APSUSC.2016.11.202.

[70] L. Liu *et al.*, “Oxygen vacancies: The origin of n-type conductivity in ZnO,” *Physical Review B*, vol. 93, no. 23, Jun. 2016, doi: 10.1103/PHYSREVB.93.235305.

[71] S. S. Kulkarni, S. Sawarkar Mahavidyalaya, and M. D. Shirsat, “Optical and Structural Properties of Zinc Oxide Nanoparticles,” *International Journal of Advanced Research in Physical Science (IJARPS*, vol. 2, no. 1, p. 2349, 2015, Accessed: Jun. 14, 2022. [Online]. Available: www.arcjournals.org

[72] P. Judith Perez Espitia, N. de Fátima Ferreira Soares, J. Sélia dos Reis Coimbra, N. José de Andrade, R. Souza Cruz, and E. Antonio Alves Medeiros, “Zinc Oxide Nanoparticles: Synthesis, Antimicrobial Activity and Food Packaging Applications”, doi: 10.1007/s11947-012-0797-6.

[73] N. Serpone, D. Dondi, and A. Albini, “Inorganic and organic UV filters: Their role and efficacy in sunscreens and suncare products,” *Inorganica Chimica Acta*, vol. 360, no. 3, pp. 794–802, Feb. 2007, doi: 10.1016/J.ICA.2005.12.057.

[74] S. Talam, S. R. Karumuri, and N. Gunnam, "Synthesis, Characterization, and Spectroscopic Properties of ZnO Nanoparticles," *ISRN Nanotechnology*, vol. 2012, pp. 1–6, May 2012, doi: 10.5402/2012/372505.
[75] B. Zhang *et al.*, "Poly(Glycidyl Methacrylates)-grafted Zinc Oxide Nanowire by Surface-initiated Atom Transfer Radical Polymerization," *Nano-Micro Letters 2010 2:4*, vol. 2, no. 4, pp. 285–289, Jan. 2011, doi: 10.1007/BF03353856.
[76] W. H. Suh, K. S. Suslick, G. D. Stucky, and Y.-H. Suh, "Nanotechnology, nanotoxicology, and neuroscience," 2008, doi: 10.1016/j.pneurobio.2008.09.009.
[77] R. Guan, T. Kang, F. Lu, Z. Zhang, H. Shen, and M. Liu, "Cytotoxicity, oxidative stress, and genotoxicity in human hepatocyte and embryonic kidney cells exposed to ZnO nanoparticles," 2012, doi: 10.1186/1556-276X-7-602.
[78] R. H. J. Hannink and A. J. Hill, "Nanostructure control of materials," p. 344, 2006.
[79] T. C. Bharat, Shubham, S. Mondal, H. S. Gupta, P. K. Singh, and A. K. Das, "Synthesis of Doped Zinc Oxide Nanoparticles: A Review," *Materials Today: Proceedings*, vol. 11, pp. 767–775, Jan. 2019, doi: 10.1016/J.MATPR.2019.03.041.
[80] S. S. Kumar, P. Venkateswarlu, V. R. Rao, and G. N. Rao, "Synthesis, characterization and optical properties of zinc oxide nanoparticles," *International Nano Letters 2013 3:1*, vol. 3, no. 1, pp. 1–6, May 2013, doi: 10.1186/2228-5326-3-30.
[81] J. N. Hasnidawani, H. N. Azlina, H. Norita, N. N. Bonnia, S. Ratim, and E. S. Ali, "Synthesis of ZnO Nanostructures Using Sol-Gel Method," *Procedia Chemistry*, vol. 19, pp. 211–216, Jan. 2016, doi: 10.1016/J.PROCHE.2016.03.095.
[82] X. Jin *et al.*, "Bright alloy type-II quantum dots and their application to light-emitting diodes," *Journal of Colloid and Interface Science*, vol. 510, pp. 376–383, Jan. 2018, doi: 10.1016/J.JCIS.2017.09.080.
[83] A. Alexandrov, M. Zvaigzne, D. Lypenko, I. Nabiev, and P. Samokhvalov, "Al-, Ga-, Mg-, or Li-doped zinc oxide nanoparticles as electron transport layers for quantum dot light-emitting diodes," *Scientific Reports 2020 10:1*, vol. 10, no. 1, pp. 1–11, May 2020, doi: 10.1038/s41598-020-64263-2.
[84] Y. Tang *et al.*, "Low-temperature solution processed flexible silver nanowires/ZnO composite electrode with enhanced performance and stability," *Journal of Alloys and Compounds*, vol. 747, pp. 659–665, May 2018, doi: 10.1016/J.JALLCOM.2018.03.083.
[85] I. N. Kashkool, V. P. Afanasjev, and N. v. Mukhin, "Electrical and optical properties of ZnO, CuO thin films and fabrication of (ZnO/CuO) heterojunction solar cell by thermal treatment," *Journal of Physics: Conference Series*, vol. 1879, no. 3, p. 032114, May 2021, doi: 10.1088/1742-6596/1879/3/032114.
[86] D. C. Choo and T. W. Kim, "Degradation mechanisms of silver nanowire electrodes under ultraviolet irradiation and heat treatment," *Scientific Reports 2017 7:1*, vol. 7, no. 1, pp. 1–12, May 2017, doi: 10.1038/s41598-017-01843-9.
[87] F. P. García De Arquer, F. J. Beck, M. Bernechea, and G. Konstantatos, "Plasmonic light trapping leads to responsivity increase in colloidal quantum dot photodetectors," *Applied Physics Letters*, vol. 100, no. 4, p. 043101, Jan. 2012, doi: 10.1063/1.3678039.
[88] C. R. Kagan, L. C. Bassett, C. B. Murray, and S. M. Thompson, "Colloidal Quantum Dots as Platforms for Quantum Information Science," *Chemical*

Reviews, vol. 121, no. 5, pp. 3186–3233, Mar. 2021, doi: 10.1021/ACS.CHEMREV.0C00831.

[89] K. S. Leck *et al.*, "Quantum dot light-emitting diode with quantum dots inside the hole transporting layers," *ACS Applied Materials and Interfaces*, vol. 5, no. 14, pp. 6535–6540, Jul. 2013, doi: 10.1021/AM400903C/SUPPL_FILE/AM400903C_SI_001.PDF.

[90] Q. Zhao *et al.*, "Colloidal Quantum Dot Solar Cells: Progressive Deposition Techniques and Future Prospects on Large-Area Fabrication," *Advanced Materials*, vol. 34, no. 17, p. 2107888, Apr. 2022, doi: 10.1002/ADMA.202107888.

[91] P. M. Pataniya, B. M. Soni, G. K. Solanki, V. Patel, and C. K. Sumesh, "Photodetector based on liquid phase exfoliated SnSe quantum dots," *Opt Mater (Amst)*, vol. 125, p. 112110, Mar. 2022, doi: 10.1016/J.OPTMAT.2022.112110.

[92] F. Grillot, W. W. Chow, B. Dong, S. Ding, H. Huang, and J. Bowers, "Multimode Physics in the Mode Locking of Semiconductor Quantum Dot Lasers," *Applied Sciences 2022, Vol. 12, Page 3504*, vol. 12, no. 7, p. 3504, Mar. 2022, doi: 10.3390/APP12073504.

[93] M. Liu, N. Yazdani, M. Yarema, M. Jansen, V. Wood, and E. H. Sargent, "Colloidal quantum dot electronics," 1928, doi: 10.1038/s41928-021-00632-7.

[94] "Quantum Dots - Articles & Publications - Blog | Quantum Solutions." https://quantum-solutions.com/blog/quantum-dots/ (accessed Jul. 26, 2022).

[95] Q. A. AKKERMAN, "Lead Halide Perovskite Nanocrystals: A New Age of Semiconductive Nanocrystals," Mar. 2019, doi: 10.15167/AKKERMAN-QUINTEN-ADRIAAN_PHD2019-03-14.

[96] S. v. Gaponenko, "Introduction to nanophotonics," *Introduction to Nanophotonics*, pp. 1–465, Jan. 2010, doi: 10.1017/CBO9780511750502.

[97] G. Wei, D. A. Czaplewski, E. J. Lenferink, T. K. Stanev, I. Woong Jung, and N. P. Stern, "Size-tunable Lateral Confinement in Monolayer Semiconductors", doi: 10.1038/s41598-017-03594-z.

[98] "Quantum Dot Absorbance, Photoluminescence Spectra and Lifetimes", Accessed: Jul. 26, 2022. [Online]. Available: https://www.thermofisher.com/order/catalog/product/Q25021MP

[99] "Module-2: Excitons and excitonic Bohr radius, energy levels, splitting 1.1 Semiconductors and excitons".

[100] O. Chen *et al.*, "Compact high-quality CdSe-CdS core-shell nanocrystals with narrow emission linewidths and suppressed blinking," *Nat Mater*, vol. 12, no. 5, pp. 445–451, May 2013, doi: 10.1038/NMAT3539.

[101] H. Shen *et al.*, "Visible quantum dot light-emitting diodes with simultaneous high brightness and efficiency," *Nature Photonics*, doi: 10.1038/s41566-019-0364-z.

[102] A. Valizadeh *et al.*, "Quantum dots: synthesis, bioapplications, and toxicity," 2012, doi: 10.1186/1556-276X-7-480.

[103] D. Bera, L. Qian, T.-K. Tseng, and P. H. Holloway, "Quantum Dots and Their Multimodal Applications: A Review," *Materials*, vol. 3, pp. 2260–2345, 2010, doi: 10.3390/ma3042260.

[104] D. Leonard, M. Krishnamurthy, C. M. Reaves, S. P. Denbaars, and P. M. Petroff, "Direct formation of quantum-sized dots from uniform coherent islands of InGaAs on GaAs surfaces," *Applied Physics Letters*, vol. 63, no. 23, p. 3203, Aug. 1998, doi: 10.1063/1.110199.

[105] K. Leonardi *et al.*, "Formation of self-assembling II–VI semiconductor nanostructures during migration enhanced epitaxy," *Journal of Crystal Growth*, vol. 184–185, pp. 259–263, Feb. 1998, doi: 10.1016/S0022-0248(98)80055-9.
[106] M. T. Swihart, "Vapor-phase synthesis of nanoparticles," *Current Opinion in Colloid & Interface Science*, vol. 8, no. 1, pp. 127–133, Mar. 2003, doi: 10.1016/S1359-0294(03)00007-4.
[107] E. Kurtz *et al.*, "Formation and properties of self-organized II-VI quantum islands," *Thin Solid Films*, vol. 367, no. 1–2, pp. 68–74, May 2000, doi: 10.1016/S0040-6090(00)00665-9.
[108] S. H. Xin *et al.*, "Formation of self-assembling CdSe quantum dots on ZnSe by molecular beam epitaxy," *Applied Physics Letters*, vol. 69, no. 25, p. 3884, Jun. 1998, doi: 10.1063/1.117558.
[109] Y. Altintas, S. Genc, M. Y. Talpur, and E. Mutlugun, "CdSe/ZnS quantum dot films for high performance flexible lighting and display applications," *Nanotechnology*, vol. 27, no. 29, p. 295604, Jun. 2016, doi: 10.1088/0957-4484/27/29/295604.
[110] L. Dou *et al.*, "Solution-processed hybrid perovskite photodetectors with high detectivity," *Nature Communications 2014 5:1*, vol. 5, no. 1, pp. 1–6, Nov. 2014, doi: 10.1038/ncomms6404.
[111] I. K. Kim, J. H. Jo, B. (Jinwoo) Lee, and Y. J. Choi, "Detectivity analysis for organic photodetectors," *Organic Electronics*, vol. 57, pp. 89–92, Jun. 2018, doi: 10.1016/J.ORGEL.2018.02.036.
[112] X. Li *et al.*, "High Detectivity Graphene-Silicon Heterojunction Photodetector," 2015, doi: 10.1002/smll.201502336.
[113] X. Gong *et al.*, "High-detectivity polymer photodetectors with spectral response from 300 nm to 1450 nm," *Science (1979)*, vol. 325, no. 5948, pp. 1665–1667, Sep. 2009, doi: 10.1126/SCIENCE.1176706/SUPPL_FILE/PAP.PDF.
[114] S. Cakmakyapan, P. K. Lu, A. Navabi, and M. Jarrahi, "Gold-patched graphene nano-stripes for high-responsivity and ultrafast photodetection from the visible to infrared regime," *Light: Science & Applications 2018 7:1*, vol. 7, no. 1, pp. 1–9, Jun. 2018, doi: 10.1038/s41377-018-0020-2.
[115] N. Gasparini *et al.*, "Visible and Near-Infrared Imaging with Nonfullerene-Based Photodetectors," *Advanced Materials Technologies*, vol. 3, no. 7, p. 1800104, Jul. 2018, doi: 10.1002/ADMT.201800104.
[116] S. Siontas, D. Li, H. Wang, A. A.V.P.S, A. Zaslavsky, and D. Pacifici, "High-performance germanium quantum dot photodetectors in the visible and near infrared," *Materials Science in Semiconductor Processing*, vol. 92, pp. 19–27, Mar. 2019, doi: 10.1016/J.MSSP.2018.03.024.
[117] W. Deng *et al.*, "Ultrahigh-Responsivity Photodetectors from Perovskite Nanowire Arrays for Sequentially Tunable Spectral Measurement," *Nano Lett*, vol. 17, p. 41, 2017, doi: 10.1021/acs.nanolett.7b00166.
[118] K. Xu, W. Zhou, Z. Ning, K. Xu, W. Zhou, and Z. Ning, "Integrated Structure and Device Engineering for High Performance and Scalable Quantum Dot Infrared Photodetectors," *Small*, vol. 16, no. 47, p. 2003397, Nov. 2020, doi: 10.1002/SMLL.202003397.
[119] W. Tang *et al.*, "MoS 2 nanosheet photodetectors with ultrafast response," *Citation: Appl. Phys. Lett*, vol. 111, p. 153502, 2017, doi: 10.1063/1.5001671.
[120] N. Das, A. Karar, M. Vasiliev, C. L. Tan, K. Alameh, and Y. T. Lee, "Analysis of nano-grating-assisted light absorption enhancement in metal–semiconductor–metal photodetectors patterned using focused ion-beam lithography," *Optics*

Communications, vol. 284, no. 6, pp. 1694–1700, Mar. 2011, doi: 10.1016/J.OPTCOM.2010.11.065.
[121] X. Zhou *et al.*, "Ultrathin SnSe2 Flakes Grown by Chemical Vapor Deposition for High-Performance Photodetectors," *Advanced Materials*, vol. 27, no. 48, pp. 8035–8041, Dec. 2015, doi: 10.1002/ADMA.201503873.
[122] C. H. Lin and R. Chen, "Ultrasonic nanoimprint lithography: a new approach to nanopatterning," *https://doi.org/10.1117/1.2172992*, vol. 5, no. 1, p. 011003, Jan. 2006, doi: 10.1117/1.2172992.
[123] Y. Berencén *et al.*, "Room-temperature short-wavelength infrared Si photodetector," *Scientific Reports 2017 7:1*, vol. 7, no. 1, pp. 1–9, Mar. 2017, doi: 10.1038/srep43688.
[124] T. P. Sidiki and C. M. S. Torres, "Silicon-Based Optoelectronics: Progress and Challenges," *Tr. J. of Physics*, vol. 23, p. 665, 1999.

CURRICULUM VITAE

Education:

2015 – 2019 B.Sc., Eletrical and Electronics Engineering, Erciyes University, Kayseri, TURKEY

2020 – Present M.Sc., Electrical and Computer Engineering, Abdullah Gul University, Kayseri, TURKEY

International Conferences:

1. M. Savas, A. F. Yazici, A. Arslan, E. Mutlugün, and T. Erdem, "Simple, sustainable fabrication of fully solution-processed, transparent, metal-semiconductor-metal photodetectors using a surgical blade as an alternative to conventional tools," *https://doi.org/10.1117/12.2621385*, vol. 12131, pp. 181–193, May 2022, doi: 10.1117/12.2621385.